SEARCH FOR AXION-LIKE PARTICLES IN THE SLAC BEAM DUMP

by

Bin Lu

Dissertation submitted to the Faculty of the
Virginia Polytechnic Institute and State University
in partial fulfillment of the requirements for the degree of

DOCTOR OF PHILOSOPHY

in

Physics

APPROVED:

Luke. W. Mo, Chairman

Silverio P. Almeida

Richard A. Arndt

Thomas E. Gilmer, Jr.

Robert E. Marshak

July, 1987

Blacksburg, Virginia

SEARCH FOR AXION-LIKE PARTICLES IN THE SLAC BEAM DUMP

by

Bin Lu

Committee Chairman: Luke W. Mo

Physics

(ABSTRACT)

A search for axion-like particles was made at the Stanford Linear Accelerator Center (SLAC) by dumping 30 Coulombs of 20 GeV electrons into a beam absorption facility. After 179 meters of earth shielding the in-flight decay of the particle into two photons or an electron-positron pair, in a decay volume of 204 meters in length, was searched for with a fine-grained electromagnetic calorimeter. No positive signals were identified. Experimental limits were obtained for axions of mass up to $\sim 200\ MeV/c^2$, and photinos of mass up to $\sim 65\ MeV/c^2$.

Acknowledgements

Today a high energy physics experiment is not a one man task, it involves a large number of people equipped with knowledge in different fields. Firstly, I would like to thank all the collaboration members who prepared and ran this experiment. They are J. D. Bjorken, S. Ecklund, W. R. Nelson, A. Abashian, C. Church, L. W. Mo, T. Nunamaker, and P. Rassmann. I would like especially to thank my advisor Professor Luke W. Mo, spokesman of this experiment, who introduced me to the field of high energy physics and guided me to the completion of my study. I would also like to thank

with whom I did the data analysis, and

for reading the draft of this dissertation and making suggestions. I record here my gratitude to for her thoughtful help throughout my graduate study. I would like to acknowledge the support of the National Science Foundation for this experiment under grant PHY-8607801 without which the experiment, and the opportunity of my participation in it, would have been impossible. Finally I would like to express my thanks to my parents who love physics and encourage me to study it.

Table of Contents

List of Figures

Chapter I

Introduction

During the past decades, high energy physicists have found many elementary particles, which appear to be the smallest building blocks of the universe. Although the table of these elementary particles is well organized, it may not be complete and it is still very important to search for new ones. In this thesis we shall describe a beam dump experiment, E137, performed at the Standford Linear Accelerator Center (SLAC). This experiment was designed to search for axion-like particles[1]; it turned out that it was also sensitive to low mass photinos[2].

It has been realized, both experimentally and theoretically, that quantum chromodynamics (QCD)[3] is a good candidate as the theory of strong interactions. A multitude of experimental results in hadronic and leptonic reactions can all be correctly accounted for by QCD[4]. However, there is no natural mechanism in the theory to preserve both parity P and time-reversal T symetries[5]. Since both P and T are experimentally known to be conserved in strong interactions[6], this strong P and T problem in QCD has to be resolved in some reasonable manner. One logical way out of this

dilemma is to introduce an "axion" particle through the breaking of the Peccei-Quinn symmetry[7,8,9], which we will describe briefly below.

QCD is constructed from the Yang-Mills fields[10], and it has a P and T violation term given by

$$i\theta \frac{g^2}{32\pi^2} F^a_{\mu\nu} \tilde{F}^{\mu\nu}_a, \tag{I.1}$$

where $F^a_{\mu\nu}$ is the gauge field strength, θ is a parameter which labels the strength of P and T violations and g is the coupling constant of the gauge field. It is analogous to $\vec{E} \cdot \vec{B}$ in electromagnetism, which violates P and T. Peccei and Quinn have observed that a rotation of the fermion fields simply produces a term proportional to the strong P and T violation term in QCD (i.e. the rotation will change the value of θ) if all the fermions are massless. Therefore, it is hopeful to solve the strong P and T problem if the QCD lagrangian possesses a symmetry which allows a rotation of the fermion fields to change the magnitude of the strong P and T violation term without changing other physics, and if this symmetry can be broken in such a manner that a small P and T violation term can be obtained. This method is known as the Peccei-Quinn mechanism[7]. The symmetry is introduced by coupling fermions to a pseudo-scalar particle. It is broken spontaneously by a non-zero vacuum value of the scalar field. This procedure is in analogy to the one employed in the standard electroweak model[11]. After the spontaneous symmetry breaking the strong P and T violation term is removed by redefinition of the fields, to give masses to fermions. In this model the strong P and T are thus made conserved.

It was pointed out by Wilczek[8] and Weinberg[9] that there must exist

a pseudo-scalar particle, named an axion, resulting from this Peccei-Quinn mechanism. These authors have observed that the Peccei-Quinn symmetry is not an exact one, because the rotation of the fermion fields also changes the magnitude of the P and T violation term (i.e. the symmetry is also broken explicitly). Therefore, according to Wilczek and Weinberg, the axion must acquire a mass. Since the axion is a pseudo-scalar particle it can decay into two photons. If its mass is heavier than twice that of leptons it can also decay into a e^+e^- or $\mu^+\mu^-$ pair.

The Peccei-Quinn-Wilczek-Weinberg (PQWW) axion has been ruled out by a number of axion-search experiments[12-22]. But it is still important to continue generic searches for this class of particle without reference to any specific theoretical model[1,23]. The axion-like particles are assumed to have the same decay channels as the classical PQWW axions. We may consider that the axion-like particle can only couple to photons and leptons but not to quarks. In order to answer this question, the experiment E137 at SLAC was proposed. It was a 20 GeV electron beam dump experiment. When the 20 GeV electron beam was dumped into a beam absorption facility, it generated an electromagnetic shower consisting of electrons, positrons and photons. These photons and electrons in the shower would interact with beam dump material again to produce axion-like particles through the production mechanism of either the Primakoff effect[24] or axion bremsstrahlung[25], respectively. It was also assumed that axion-like particles are sufficiently long lived in order to penetrate the shielding and to decay into a pair of photons or a pair of electrons in the

air space between the down stream end of the beam dump and the detector. This experiment was designed to detect the decay products from axion-like particles with a fine-grained electromagnetic calorimeter. Owing to the collimation of the electromagnetic shower[26] and the collimation of axion-like particle production mechanisms, the signature of an axion-like particle would be a pair of photons or electrons with very small angles with respect to the primary electron beam direction.

I.1 Review of Axion Search Experiments

The axion-like particle is characterized by its mass m_X and its decay coupling constant F_X. For pseudo-scalar particles, the decay coupling constant is usually described by the partially conserved axial current theorem (PCAC),

$$\partial_\mu A^\mu = F_X \phi_X, \tag{I.2}$$

where A^μ is the axial current, and ϕ_X is the axion-like particle field. Since there is no definite information on the axion-like particle, both F_X and m_X are regarded as free parameters. In the situation of negative experimental results, the excluded region of the parameter space $F_X - m_X$ can be determined.

A number of experiments have already been carried out to search for this generic type of axion[27-29]. These experiments together with PQWW axion search experiments can be categorized as follows:

1. **The reactor experiments.** The axions are assumed to be produced in the decays of excited fission products. The first result is from

the Savannah River reactor[12,22]. The most likely signals were the photons from the decay process $X \rightarrow 2\gamma$, or recoil electrons or photons from the reaction $X + e \rightarrow \gamma + e$. The second result is from the ILL reactor at Grenoble[17]. There a search for coincident gamma-ray events from the decay of an axion into two photons has been performed. This experiment covered the axion mass region up to 280 KeV/c^2.

2. **Radiative decay of ψ and Υ.** The particles ψ and Υ are assumed to be able to decay into axions along with photons[8,9]. The ψ radiative decay experiment was done at SPEAR of SLAC with the Crystal Ball detector[13]. The experiment was sensitive to axions of mass less than 1 GeV/c^2. There are three Υ radiative decay experiments: two were performed at the Cornell Electron Storage Ring (CESR) with the CUSB detector[14] and the CLEO detector[15], and the third at DORIS with the LENA detector[16]. The CUSB experiment excluded the axion with mass up to 7 GeV/c^2.

3. **The nuclear transition experiment.** The search for axion emission in the decay of excited states of ^{12}C in M1 transitions was carried out at the Princeton University cyclotron[18]. The experiment was sensitive to the axion with mass between 1 and 15 MeV/c^2 decaying into two electrons. A search for axion emission in ^{137}Ba was performed at the Swiss Federal Institute of Technology[19]. It was sensitive to the two-photon decay mode of the axion, with its mass greater than 160 KeV/c^2.

4. **Electron beam dump experiments.** The first electron beam dump search was carried out at the Armed Forces Radiobiology Research Institute[20]. The incident electron beam energy was 45.3 MeV. The experimental signature was either a pair of photons or a pair of electrons. In analyzing the result, the axions were assumed to be produced by the process of electron bremsstrahlung[25]. Three new electron beam dump experiments were performed recently to search for axions with mass around 1.8 MeV/c^2[30]. They are SLAC experiment E141[31], the Orsay experiment[32] and the KEK-Kyoto experiment[33] with electron incident energies of 9 GeV, 1.5 GeV and 2.5 GeV, respectively.

5. **The proton and the pion beam dump experiment.** The first proton beam dump experiment was done at the Clinton P. Anderson Meson Physics Facility (LAMPF)[21] looking for the photons from axion decay. The incident energy of proton beam was 750 MeV. Higher energy proton beam dump experiments were performed at the European Organization for Nuclear Research (CERN) by the CDHS[27] and CHARM[28] groups. The proton incident energy for CHARM was 400 GeV. Both experiments looked for photons, electrons, and muons from decays of axion-like particles. In addition a pion beam dump experiment was performed by the NA3 collaboration[29] at the CERN SPS. The π^- incident energy was 300 GeV. The experiment was sensitive to the two-photon decay mode of the axion-like particle. In the data analyses of the above three experiments the axion-like

particles were assumed to couple to nucleons in the same manner as does the pion, and to be produced through the mixing of axions with pions. The experimental limits given by the CDHS and CHARM are very close to the limits obtained from the SLAC E137 experiment. Results of the three experiments are compared in Chapter IV. The most recent proton beam dump experiment to search for axions was done at Fermi National Accelerator Laboratory (Fermilab)[34]. This experiment looked for electron pairs from the decays of the 1.8 MeV axions[30]. The axion production mechanism was assumed to be bremsstrahlung of axions by electrons in the hadronic shower initiated by the 800 GeV proton. The axion mass range covered was from 1 to 16 MeV/c^2.

In the ψ and Υ radiative decay experiments, the axion was assumed to couple to heavy quarks[8,9]. The relative rate for production of an axion in the radiative decay of a heavy vector meson made up of either charge $2/3$ or $-1/3$ quarks is proportional to the quark mass squared. Moreover, the rate associated with charge $2/3$ quarks is proportional to x^2, while that of charge $-1/3$ quarks is proportional to x^{-2}, where x is a symmetry breaking parameter in the PQWW axion model. Therefore, the product of the branching ratios of ψ and Υ radiative decays into axions is proportional to the c-quark mass squared and b-quark mass squared, but is independent of the unknown parameter x.

In the experiments both ψ and Υ were produced by colliding electrons with positrons. Since the axion is a very weakly interacting particle, it has

a relatively long lifetime and will not decay inside the detector. As a result, the signature for either ψ or Υ decaying into an axion and a photon is a single photon in the detector. The Crystal Ball detector used in a ψ radiative decay experiment[13] was basically a spherical array of 16 radiation lengths NaI(T1) crystals which covered 98% of 4π sr. It was used to measure the photon energy and direction. Cylindrical magnetostrictive spark chambers and a multiwire proportional chamber placed around the beam pipe were used to reject the charged particles. The CUSB detector[14] used in the Υ radiative decay experiment consisted of 8 radiation lengths of NaI crystals, which covered 90% of 4π sr, backed up by 7 radiation lengths of lead glass. Drift chambers before the NaI provided tracking information for charged particles, while cathode-readout proportional chambers interleaved between the radial NaI layers provided tracking information for photons. The product of the branching ratios of ψ and Υ radiative decays was measured to be 0.6×10^{-9} in these experiments, which is inconsistent with the theoretical prediction of 1.6×10^{-8}. The PQWW axion with mass less than 1 GeV/c^2 is, therefore, convincingly ruled out by the two experiments.

To search for a new particle implicated in a theory, it is important to look for it in many possible ways. The results in experiments with hadron beams have been turned out to be negative. There might be a possibility that an axion can only couple to photons or leptons, but not to quarks. In that case, a search with high energy electron beams will be advantageous. Another distinct feature of searching for axions in the electron beam dump experiment is that the axion flux has a very sharp angular distribution

around the primary electron beam direction; were axions to exist, such a peak could be seen. The SLAC E137 is the only high energy and high luminosity electron beam dump experiment to search for this type of axion-like particle. It was sensitive to the axion mass ranging from 50 KeV/c^2 to 200 MeV/c^2. The details of the axion-like particle production mechanism and the production cross sections are given in Appendix B.

I.2 Photino

In supersymmetry models[2] each fermion is assumed to have a spin zero partner, and each boson a fermionic partner. For example, the electron has a spin zero partner, the selectron, and the photon has a spin 1/2 partner, the photino, etc. There can also exist a massless fermion of spin 1/2, the goldstino. The photino will then decay into a photon plus a goldstino[35]. If the photino exists, it might be relevant in explaining the $3°K$ background radiation of the universe. It has also been thought that both axions and photinos are the important components of dark matter in the universe[35].

Electron-positron annihilations can give rise to photinos[36]. Only photons from photinos can be seen by the detectors. The lifetime of the photino is expressed in terms of its mass and the supersymmetry breaking scale. The expression for the photino lifetime and production cross section are given in Appendix B. There are four e^+e^- colliding beam experiments at PETRA: CELLO[37], JADE[38], MARK J[39], and TASSO[40]. These experiments also searched for photinos, and were sensitive to a photino mass in the range of 10 MeV/c^2 to 20 GeV/c^2.

The SLAC E137 experiment was the first and the only electron beam dump experiment to search for the light photinos. The photinos could be produced by positrons in the electromagnetic shower when annihilating the atomic electrons in the beam dump[36]. This experiment was sensitive to the photino mass ranging from 100 KeV/c^2 to 65 MeV/c^2.

Chapter II

The Experiment

The SLAC E137 experiment was done by a collaboration of Fermilab, SLAC, and Virginia Polytechnic Institute and State University[41]. It was a search for weakly interacting objects X, which might be produced by 20 GeV electrons incident upon the SLAC beam dump. To be specific, the neutral objects we searched for were axions and photinos which could be produced by electrons, positrons and photons interacting with the beam dump material.

When the 20 GeV electron beam was dumped into the Beam Dump East of SLAC, it generated an electromagnetic shower, comprising mostly electrons, positrons and photons, in the dump. These shower particles could interact with material of the beam dump to produce the X particles. Since the X particles are supposed to couple only very weakly with ordinary matter, most of them would be able to escape the beam dump, and decay in the air space behind the dump. A fine-grained electromagnetic shower calorimeter was set up far behind the dump to observe the decay products. The electrons, positrons and photons which were produced in the dump by

the primary 20 GeV electron beam had transverse momenta less than 20 MeV/c[26]. Also, the X particles would be produced at very small angles with respect to the direction of the shower particles. For example, in the photo-production of axions through the Primakoff effect[24], axions would be produced by photons interacting with atoms in the beam dump. Since the value of the four momentum transfer to the nuclear target was very small, the angular distribution of the axions essentially followed that of the photons. Therefore, the hypothetical X particles would be produced in a well collimated beam. This results in a good acceptance for a long decay volume. It also provided an easy way to reject background, since most of the background particles were from the cosmic rays and had larger angles with respect to the primary electron beam direction.

II.1 The Experimental Layout

Figure II.1 shows the sketch of the experimental layout. Figure II.2 shows the elevation view of the beam dump and the detector location. The 20 GeV primary electron beam at SLAC was transported through End-Station A, site of the classic deep-inelastic electron scattering experiment. Then it continued through the vacuum pipe to the Beam Dump East where all the beam power was absorbed in an aluminum tank of water, and where the X particle would be produced. Beyond the Beam Dump East a hill served as an additional absorber for the known particles. The total length of the beam dump was 179 meters. The detector was located on the other side of the hill, with 204 meters of decay path between the down stream end of the

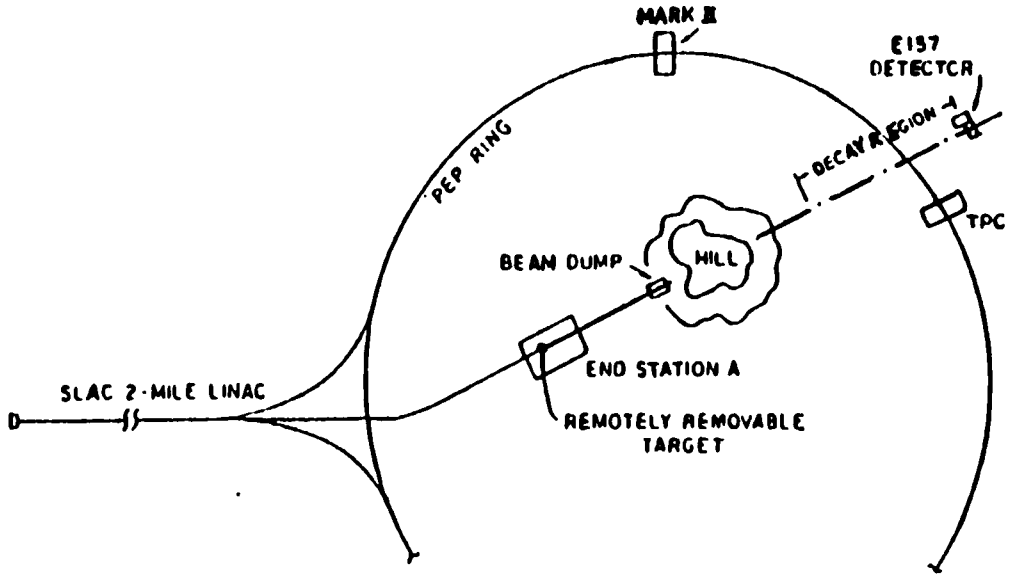

Figure II.1: Experiment layout.

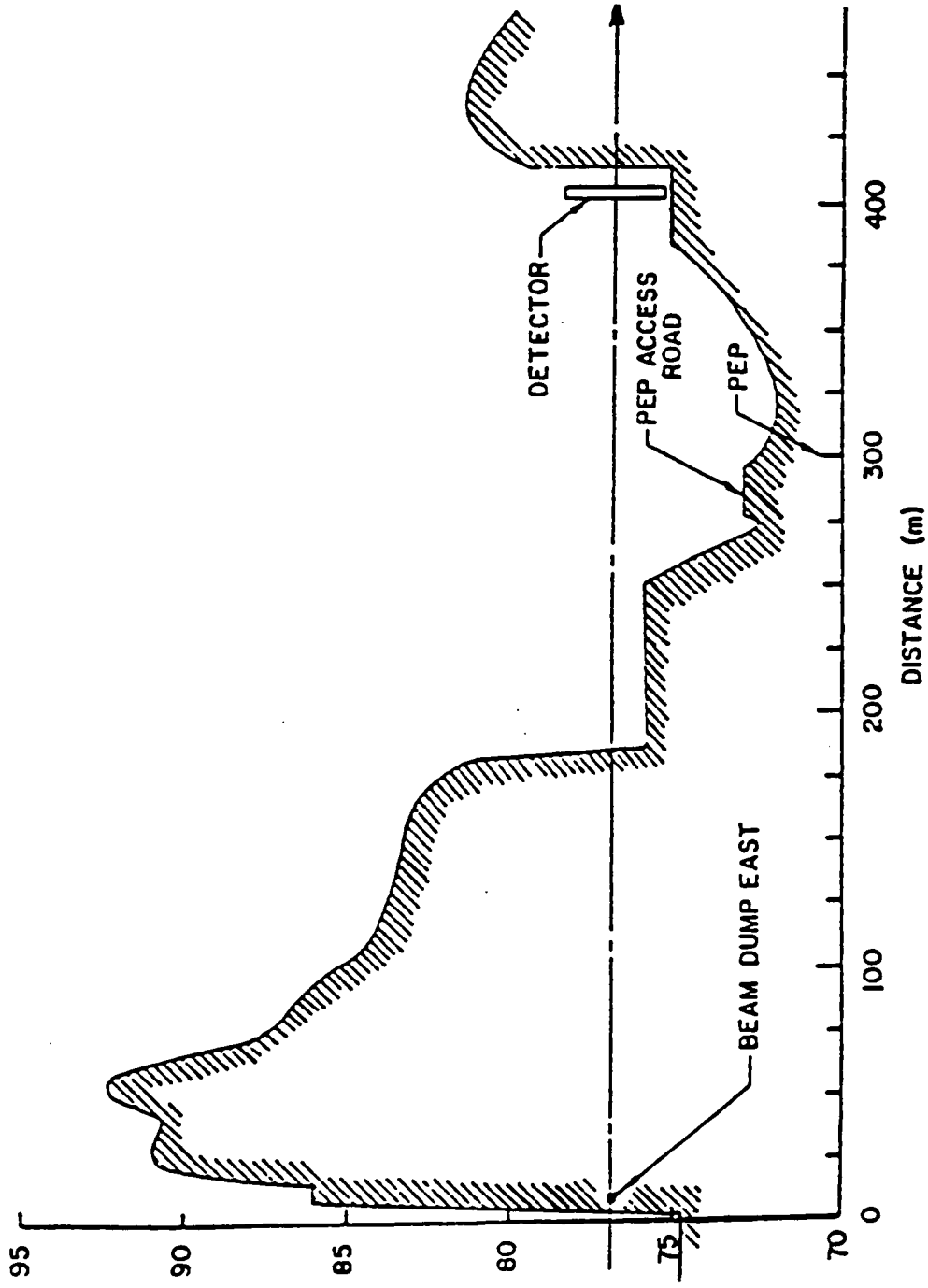

Figure II.2: Elevation view of beam dump and detector location.

dump and the detector. The approximate horizon of the shielding berm as seen by the detector was 30 mr.

II.2 The Beam and Beam Set-up

The high intensity primary beam at SLAC is quite unique. On a good day it could deliver a total of approximately 1 Coulomb of 20 GeV electrons. The 1.6 μsec pulse length and approximately 170 pulses/sec repetition rate allowed good cosmic ray rejection. For example, during the data-taking the accelerator gate width was set at 6 μsec, therefore, the duty cycle for detecting cosmic rays was less than 0.1%.

In the End Station A a remotely controlled aluminum target of various thicknesses could be inserted into the beam to generate the beam associated "skyshine" background. It was very useful for timing the electronics, setting the experimental gate, as well as for monitoring detector performance. This background was due to scattering of pions (produced by electron beam interacting with the aluminum target) from air above the top of the hill. This "skyshine" background is discussed at the end of this chapter. The target was removed during the data-taking, and the primary electron beam was transported, without changing steering, to the Beam Dump East located in the berm at the down stream end of the End Station A.

The direction and focusing of the electron beam between the End Station A and the Beam Dump East was checked with remotely controlled roller screens. The screens were coated with ZnS material and marked with a fiducial grid. The luminescence of the screen, when it was hit by

electrons, made the fine adjustment of the beam possible. After beam position adjustment, the screens were moved to a position where the beam could go through the hole on the screen without intercepting any material while taking data.

The beam transport system to End Station A acted as a double focusing spectrometer with an energy-defining slit located at the intermediate focus[42]. It is shown in Figure II.3. The switching magnet P was used to deflect the beam from the accelerator to the A Beam Line on a pulse-to-pulse basis. Two chains of bending magnets B1 and B2 were used to provide additional bending angles. B1 was also used to disperse the beam for momentum resolution at the slit. B2 was also used to separate the electron beam from the off-energy and neutral background generated at the slit. A quadrupole doublet Q1 was used to focus the beam. A quadrupole magnet Q2 was added to recollimate the beam spread out by B1 in order to bring the beam down to an acceptable diameter in the radial plane for passage through B2. Quadrupole doublets Q3 and Q4 were used to focus the beam down to the desired spot size at the target. Figure II.4 shows the envelope of the beam as it passed through the system. The envelope of the vertical plane is drawn above the center line; the horizontal plane is shown below the center line. The typical momentum spread of the beam was $\Delta p/p = 1\%$. The intensity of the beam was measured by a 33″ diameter toroidal current transformer on a pulse to pulse basis[43]. When a beam pulse went through the center of the toroid, a pulse was induced in the coil winding on the toroid. The total charge of the induced pulse was

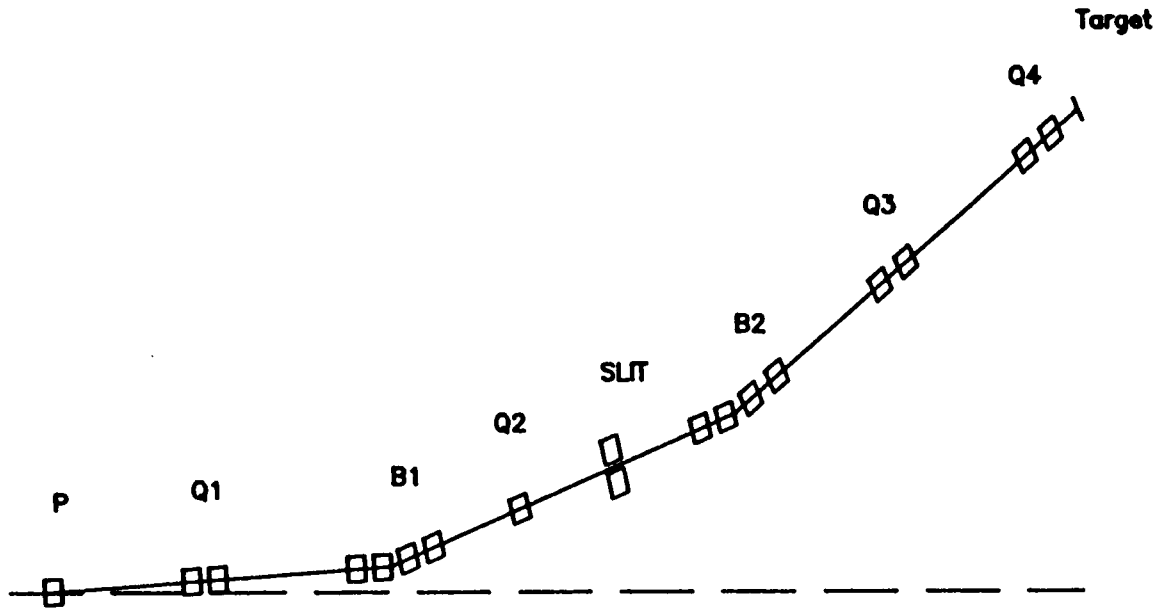

Figure II.3: Beam transport to End Station A.

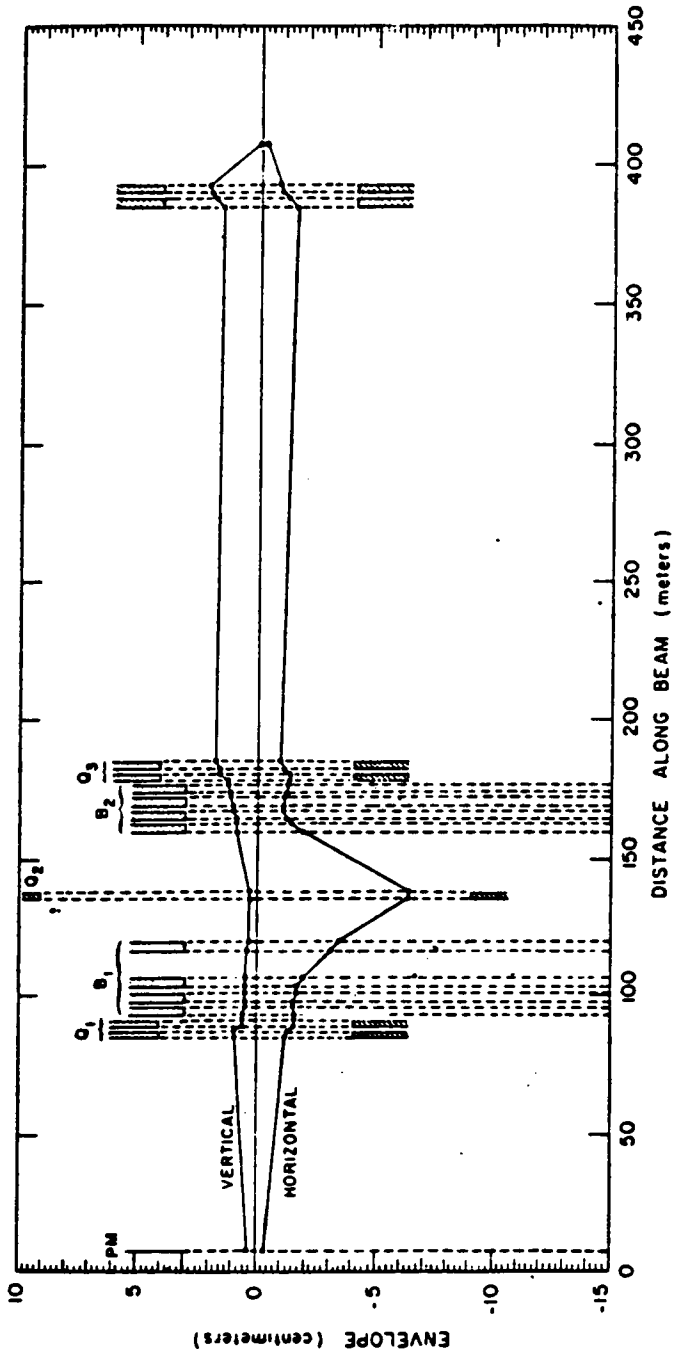

Figure II.4: The envelope of the beam as it passes through the system.

integrated and measured. It is proportional to the beam pulse that went through the center of the toroid.

II.3 The Detector

The detector was an 8-layer, one r.l. (radiation length) each, fine-grained electromagnetic shower calorimeter which was used to measure the energies and directions of the photon and electron. Each layer consisted of a hodoscope of plastic scintillation counters, one r.l. of steel or aluminum converter and one multiwire proportional chamber. The inter-chamber spacing was 15". When an electron or a photon hit the calorimeter it would generate an electromagnetic shower. The total energy of the shower was measured by the scintillation counters, and its direction was measured by the multiwire proportional chambers. For the first phase of the experiment (approximately 10 Coulombs of 20 GeV electrons dumped) the multiwire proportional chamber was a 2 $\times$ 3 mosaic of the 1 m $\times$ 1 m chambers used in the Fermilab experiment of Heisterberg et al.[44], which measured ν_μe elastic scattering. Aluminum radiator was used in this phase of the experiment. For the final phase of the experiment (approximately 20 Coulombs of 20 GeV electrons dumped) new 3 m $\times$ 3 m proportional wire chambers of similar design were installed and the radiator was replaced by one radiation length steel plates. Figure II.5 shows the schematic of the detector used in the final phase of the experiment.

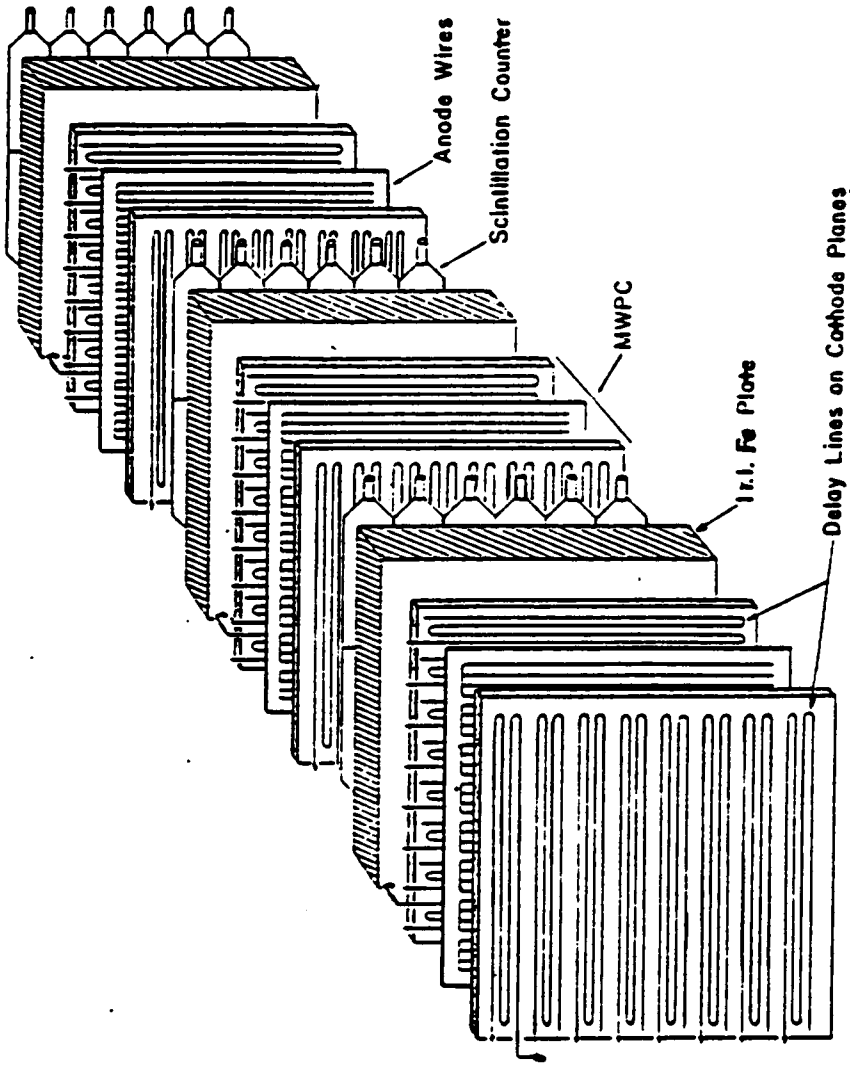

Figure II.5: Schematic arrangement of the shower detector.

II.3.1 1 m × 1 m Multiwire Proportional Chamber

Since the horizon of the shielding berm subtended an angle of only 30 mr at the detector, any particle with a vertical angle greater than 30 mr would be a background particle. It was clear that good angular resolution was essential to the experiment. This capability was obtained from the multiwire proportional chambers (MWPC). The chamber consisted of an anode wire plane and two cathode planes equipped with delay-line readouts. The schematic of the 1 $m \times 1$ m delay-line multiwire proportional chamber with readout electronics is shown in Figure II.6.

For the 48 1 m × 1 m chambers[45] the cathode plane was an aluminum plate, 1/4" thick, with a copper-clad G-10 plate glued on top of it. The G-10 plate was machine-milled into a zigzag conducting strip which served as the delay-line. The transverse spacing of the delay-line was 1.5 mm. The anode wire plane was supported by a G-10 spacer, 1/64" thick, attached to one aluminum plate. The wires were gold-plated tungsten wires of diameter 20 μm spaced 3 mm apart. The spacing between the anode plane and the cathode plane was 1/4". Figure II.7 shows the details of the chamber.

The delay-line behaved like a transmission line of $\sim$ 100 Ω impedance. When a charged particle passed through a chamber, it would ionize the gas creating pairs of electron and positive ion. The electrons had much higher mobility than the heavy ion, and therefore drifted very fast towards the anode wires. The electrons gained energy along the way in the electric field, thus ionizing more charged-pairs to provide the desired gas amplification. The total number of electrons reaching the anode was proportional

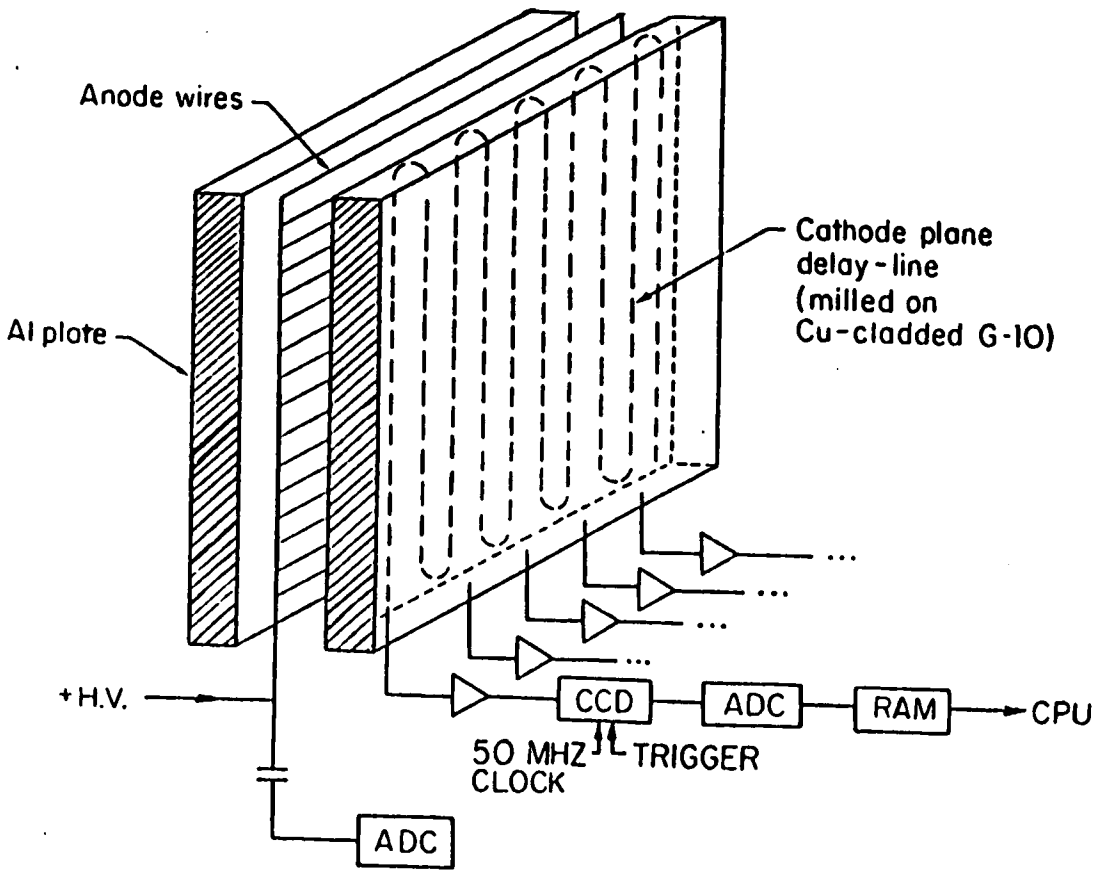

Figure II.6: Schematic of the delay-line multiwire proportional chamber and the CCD electronics.

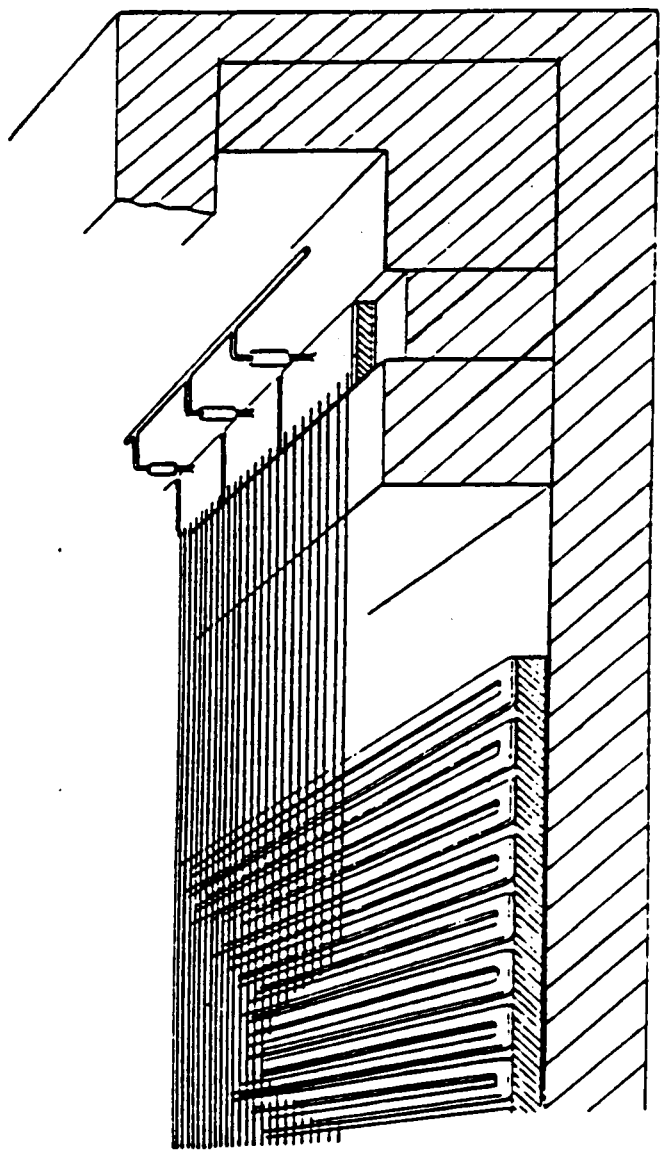

Figure II.7: Detailed arrangement of the $1m \times 1m$ MWPC.

to the number of primary ion pairs. Meanwhile, the delay-lines on the two cathode planes would also receive localized positive pulses induced by capacitive coupling. The signals would then propagate along the delay-line at a speed of about 0.2 m/nsec to the readout ports. The propagation time was recorded and later, during the data analysis, translated into the transverse track position on each cathode plane.

On each cathode plane of a chamber there were five readout ports placed equidistantly, along an edge orthogonal to the delay-line. Therefore, a delay-line was divided into four parts and every part had readout at both ends. This arrangement was necessary to take care of the signal attenuation and to provide redundancy (having signal collected at both ends); but it also introduced left-right ambiguities, which were self resolved, for the three ports in the middle. Between two neighboring ports the propagation time is about 600 nsec, corresponding to a transverse distance of 250 mm, and the signal was attenuated by about a factor of two. The dispersion and attenuation characteristics of the delay-line for a step signal are shown in Figure II.8.

The chambers were operated at a typical high voltage of $\sim$ 2800 volts on the anode planes while the cathode planes were grounded. To protect the anode wires from sparking damage, every eight anode wires were grouped together and connected to the high voltage power supply through a 10 $M\Omega$ resistor. As shown in Figure II.9 the anode wires were soldered to the G-10 spacers which acted as the high frequency coupling capacitor for the outgoing fast signal from the anode. The capacitively coupled signals collected

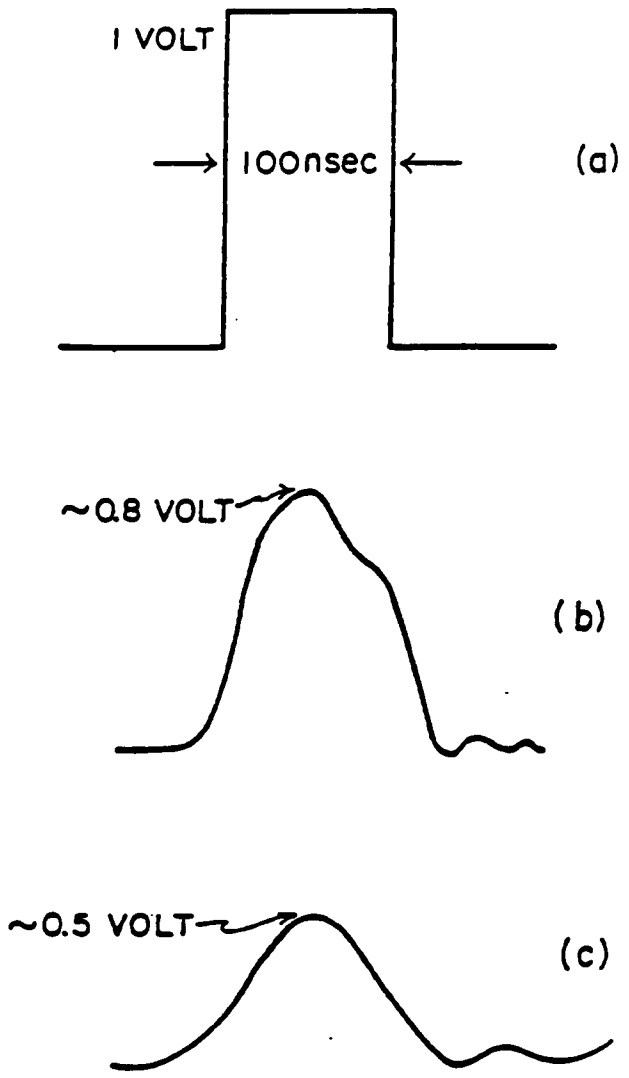

Figure II.8: The dispersion and attenuation characteristics of the delay-line for a step signal. (a) Test signal applied to the delay-line. (b) Signal after traveling half the distance between two neighboring taps. (c) Signal at the neighboring tap.

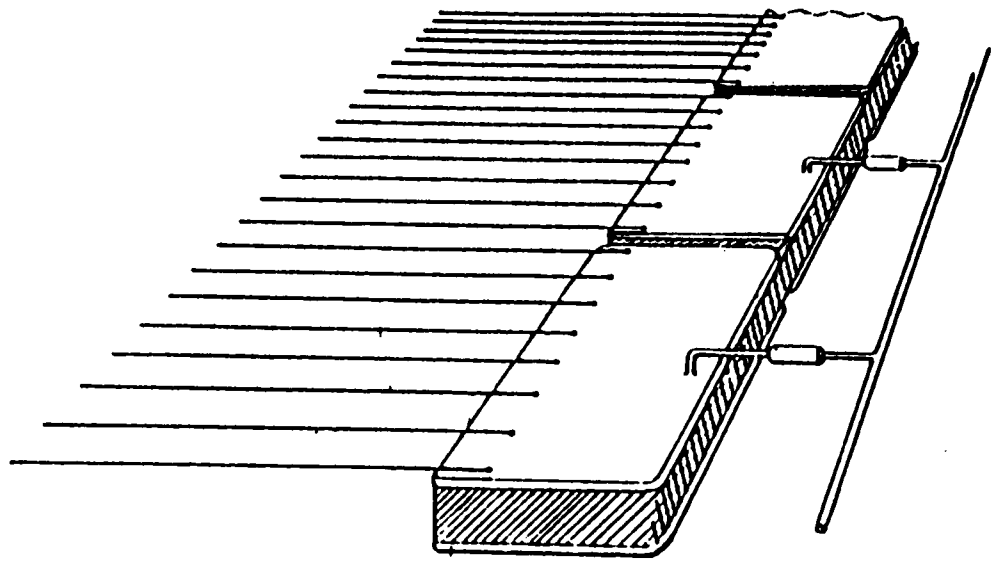

Figure II.9: Connection of anode wires to the G-10 stripe ($1m \times 1m$).

on the other side of the G-10 spacer were sent to an amplifier through a high voltage decoupling capacitor. The total pulse from the anode wires of a chamber was fed to an analog-to-digital converter (ADC) to measure the energy deposition in each layer of the detector.

The chambers were filled with a gas mixture of 80% argon, 19.7% CO_2, and 0.3% Freon-13-B1. This gas mixture is temperature-stable and could be packed into $\sim$ 2,000 psi cylinders. It has smaller amplification factor, but it has the advantage that its strong quenching effect can prevent the electromagnetic shower from spreading to allow the observation of only the "hard core" of the electromagnetic shower.

II.3.2 The CCD

As shown in Figure II.6, signals on the cathode planes would travel along the delay-lines to the tap points and be fed to the readout ports. They were first amplified by an amplifier located on the chambers, and then fed to a charge-coupled-device (CCD) through coaxial cables[1]. The operation of the CCD digitizer is shown schematically in Figure II.10. The CCD acted as an analog shift register. It was continuously clocked by a 50 MHz quartz-stabilized oscillator. Upon occurrence of each clock pulse a 20 nsec wide slice of the input signal was loaded into a CCD bucket at the front end, and the charges stored in the CCD buckets were shifted forward in sequence by one bucket. When a master experimental trigger from the scintillator hodoscope occurred, the CCD clock rate was reduced to 20 MHz until the charges in all of the CCD buckets could be read out and digitized in

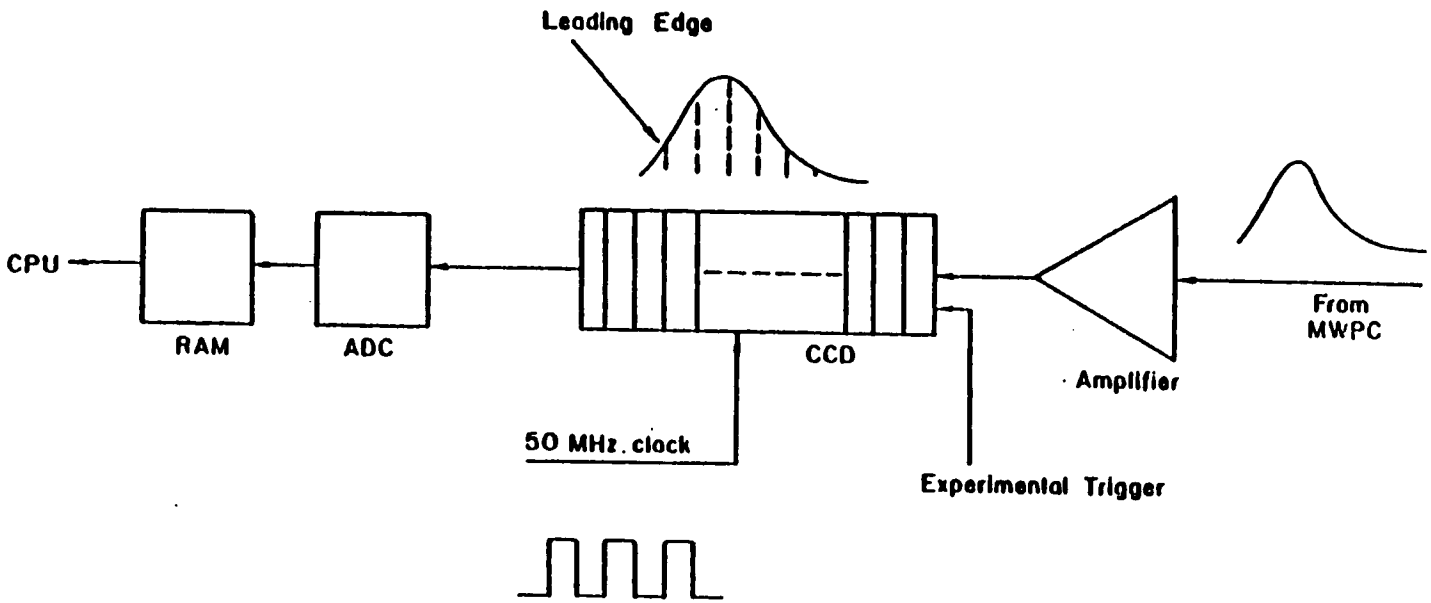

Figure II.10: Schematics of CCD digitizer

sequence by an ADC. The results were stored in the random access memory (RAM) waiting to be read into the on-line computer.

The timing of the master experimental trigger was separately recorded by using a time-to-digital converter (TDC), one on each CCD module. The TDC was started by the leading edge of each 20 nsec pulse and stopped by the trigger. The time interval between these two signals was digitized and stored in the RAM with an accuracy of 256 steps for 20 nsec. This information was used for fine-tuning of the position measurements.

The delay-line multiwire proportional chamber together with the CCD offers an elegant method of measuring both the pulse heights and track positions simultaneously. It acts like a computerized multi-beam oscilloscope. The CCD bucket number represents the track position in quantum steps of 20 nsec, and the charges in CCD buckets provide the information on pulse height distribution.

For the 1 m × 1 m MWPC, there are 32 buckets between two adjacent tap points; so each bucket represented 250 mm / 32 = 7.8 mm in real transverse space. The centroid of each shower can be determined to the accuracy of a fraction of one CCD bucket.

II.3.3 3 m × 3 m Multiwire Proportional Chamber

The eight 3 m × 3 m chambers[1] were built by the same construction method as the 1 m × 1 m chambers. The delay-line on one cathode plane was divided into 23 independent pieces, of which 22 had readout at one end only and the other ends were properly terminated to eliminate reflec-

tions. One piece of delay-line near the chamber edge had readout at both ends. This arrangement eliminated the left-right ambiguity problem for the readout ports in the middle. Examples of the pulse trains from eight of the 24 readout ports are shown in Figure II.11. It illustrates the multi-particle capability of the chamber. Thirty six CCD buckets were used for each delay-line. Therefore, one CCD bucket represent 3.6 mm in transverse space. Figure II.12 shows an event measured by 3 m $\times$ 3 m chambers. In this display, the pulse trains from all 23 sections of delay-lines on one cathode plane of a single chamber are combined together.

II.3.4 The Hodoscope

There were eight planes of scintillation counter hodoscopes. They were formed by 1.5 m $\times$ 0.5 m $\times$ 1 cm NE114 plastic scintillation counters, made by Nuclear Enterprises Inc. For the first phase of the experiment each plane consisted of eight counters; for the final phase of the experiment each plane of the hodoscope consisted of twelve counters. They were used to measure the energy deposition as well as to form the experimental trigger.

II.4 Experimental Trigger

The schematics of the fast electronics is shown in Figure II.13. The anode signal from each photomultiplier tube was first fanned out into three channels through a linear amplifier of approximately unity gain. One went to a 12-bit ADC for energy measurement. The other two signals were used to form experimental triggers.

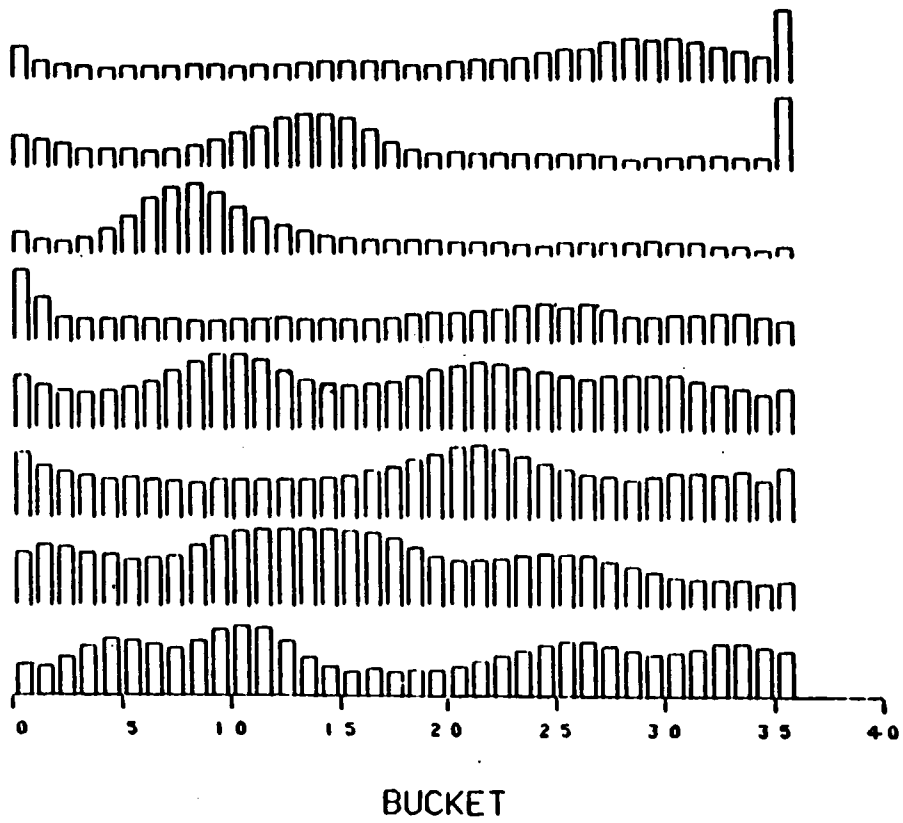

Figure II.11: Example of the CCD data from eight independent and consecutive delay-lines on one cathode plane of a $3m \times 3m$ MWPC.

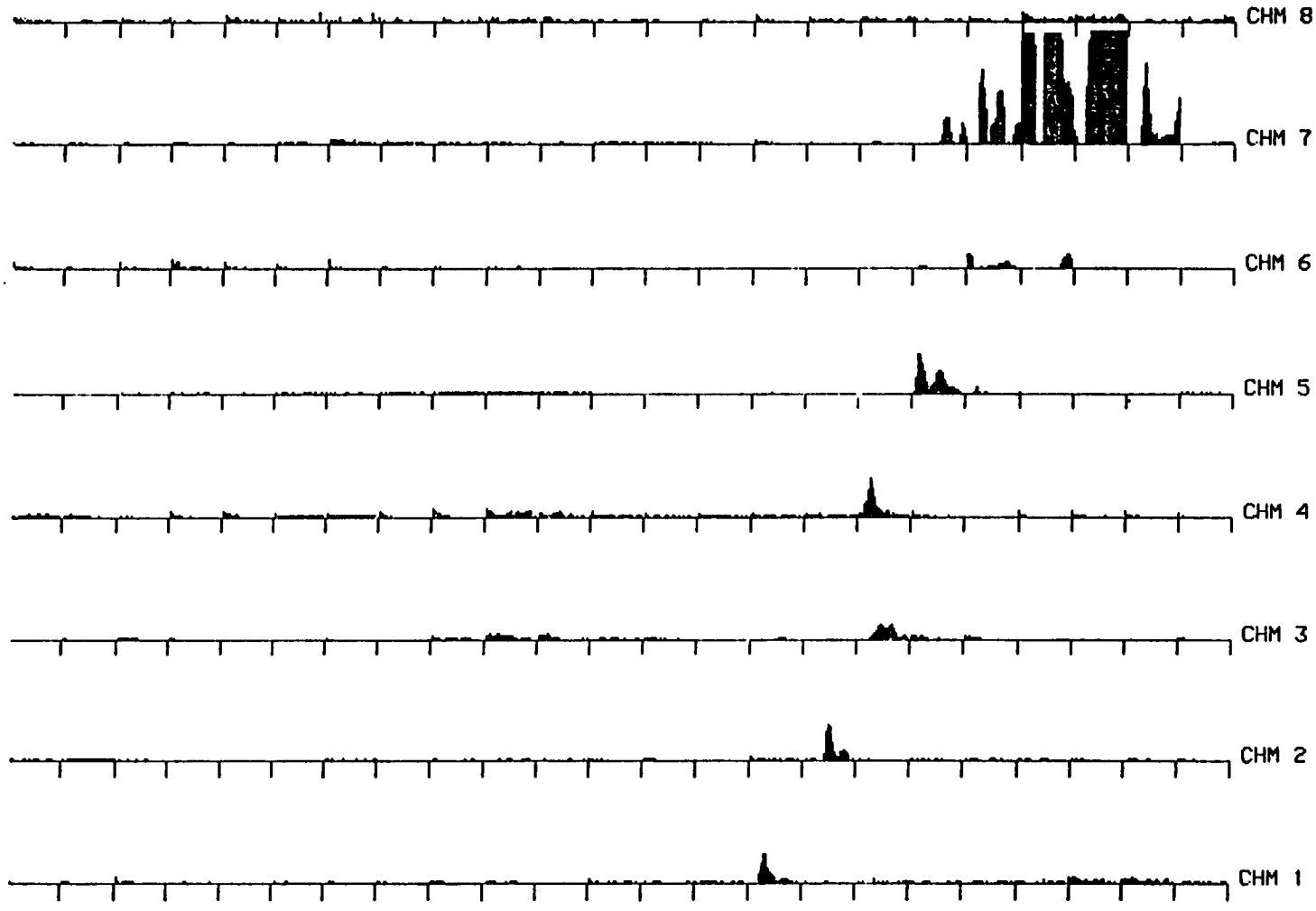

Figure II.12: An example of the CCD data from one view of eight $3m \times 3m$ MWPC's.

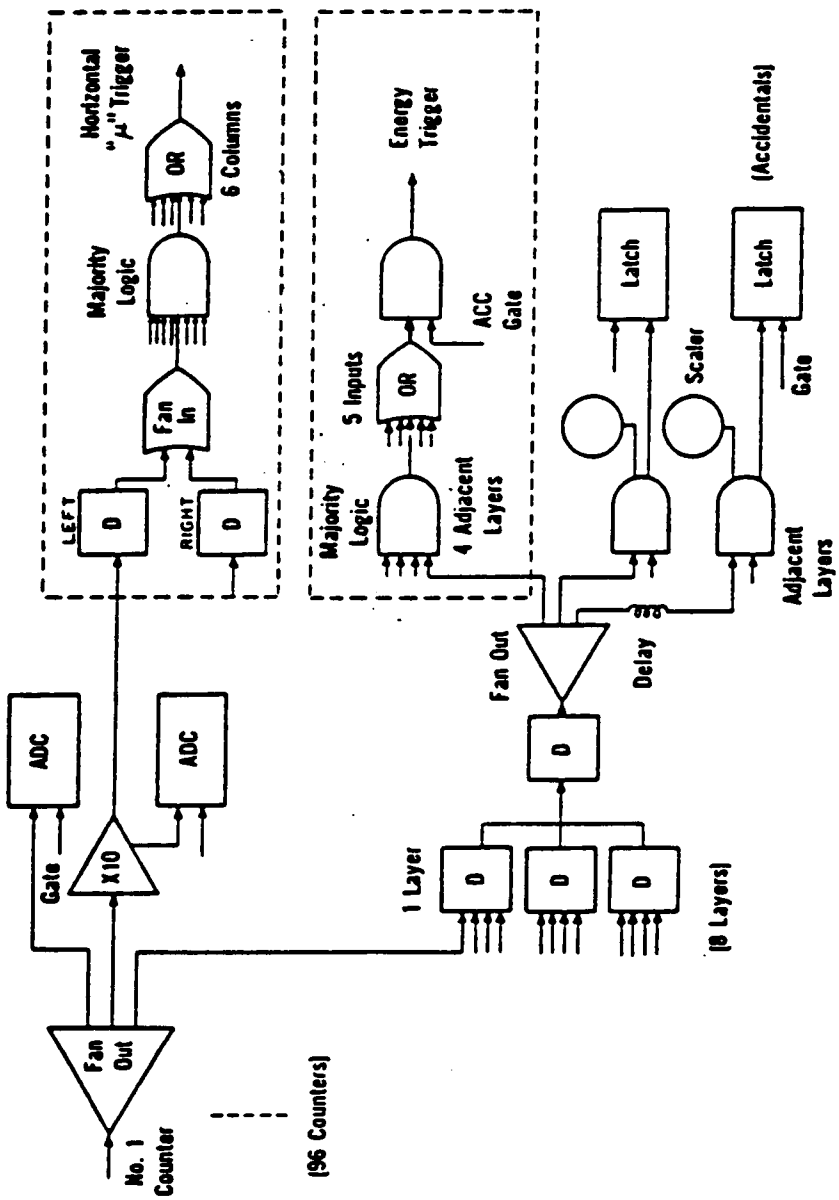

Figure II.13: Schematic of the trigger electronic.

The first trigger was a low threshold trigger, sensitive to "almost horizontal" muons. It was done as described below. The anode signal from each photomultiplier tube was first amplified by a factor of ten. The 96-element hodoscope was arranged six on the left and six on the right in a plane, and eight layers deep. The left- and right- counters in each plane at the same elevation were first combined logically together. Then they were fed into six majority logic units to form experimental triggers. Each one of the six majority logic units contained eight inputs along the beam direction. In order to ensure that the trigger was efficient for minimum ionizing particles, we further demanded that the trigger condition is given by any four of eight inputs in a given row. The outputs of the six majority logic units were "ORed" together into one output.

The second trigger employed in the experiment was an "energy threshold" trigger. All twelve counters in a single hodoscope plane were first logically summed together and then discriminated against the "energy threshold" setting of a following discriminator. The outputs from eight hodoscope planes were fed also into majority logic units. The trigger conditions were set such that if any three of four adjacent hodoscope planes passed the threshold settings, the event would be accepted.

Finally, the horizontal-muon trigger and the energy-threshold trigger were logically merged together to provide the master trigger of the experiment. The beam gate (6 μsec wide) was also applied to avoid most of the cosmic ray triggering. This arrangement not only provided selective triggering by interesting events of high energies, it also avoided possible bias

and inefficiency in the experimental trigger. As usually done, the accidental coincidence rates were monitored by coincidences with appropriate delays inserted. They were latched and also counted by scalers.

II.5 Data Acquisition System

The data acquisition system consisted of an Eclipse S/230 16-bit computer (made by Data General). The peripheral equipment consisted of a 96 MByte disk drive, a tape drive, two terminals, a printer, and a color graphics station, CGC 7900, made by Chromatics. The electronics modules, power crates, and data bus were the standard nuclear instruments and methods (NIM) computer automated measurement and control (CAMAC) system. The computer operating system was real-time disk operating system (RDOS). The data acquisition tasks were handled by a priority-interrupt scheme. Once a trigger occurred, the computer operation would be immediately interrupted to service the data acquisition routine for the experimental apparatus. Data from the CCD's, ADC's, scalers, and latches were read into the computer memory via the CAMAC interface unit, then "hard-copied" onto magnetic tapes. After the interrupt service completed, the interrupted task would be resumed. The performance of the experimental apparatus and the experimental status were monitored via graphics displays.

II.6 Calibration of Equipment

II.6.1 The Multiwire Proportional Chamber

The 49 1 m × 1 m chambers were used at Fermilab in a ν_μe elastic scattering experiment[44]. These chambers had been calibrated at Cornell University and at Fermilab using electrons of energies ranging from 2 to 30 GeV[45]. Since the calibration parameters were known the chambers were not calibrated again at SLAC. It was established that the angular resolutions of these chambers were better than 5 mr.

The eight 3 m × 3 m chambers were quite bulky. Each one weighed about 1,500 lbs. To set them up in the test beam would have been quite a job. As a result, we did not calibrate these chambers. The operating high voltage of a given chamber was set according to its response to high energy horizontal muons. Because we used these chambers only for track measurements in this experiment, this practice was adequate. The energy measurements were done using only scintillation counters.

II.6.2 Scintillation Counters

The high voltages on all 96 plastic scintillation counters were set by a procedure to be described below. Each counter was placed behind a $\sim$ 4 r.l. thick aluminum plate. A positron beam was sent through the counter at exactly the same geometric location for all counters. The high voltage on each counter was adjusted until the pulse height spectrum became identical in both magnitude and shape for all counters. At SLAC, the test beam was

the most versatile for this purpose. The beam intensity could be adjusted to a level as low as one positron per pulse and the energy could be varied from about 1 GeV to 14 GeV. With this procedure all 96 scintillation counters were set to exactly the same gain.

In February, 1984, the total energy calibrations were done on the scintillation hodoscopes using the SLAC test beam. A stack of eight counters with steel radiators, identical to that used in the experiment, was put into the electron test beam. The pulse height from each individual counter was recorded. The total energy seen by the stack was obtained by a software summation. The calibrations were done over the energy range from 1 GeV to 14 GeV. Data were also collected with the beam hitting different positions of the counters.

II.7 Experimental Procedure

The A Beam Line, End Station A, and Beam Dump East at SLAC are well-established experimental facilities. It was a pleasure to do the experiment there. On a good day, the accelerator could deliver almost one Coulomb of 20 GeV electrons to the experiment. As a result, the experimental data-taking was completed in a relatively shorted period. The experiment was proposed and approved in 1980. The first run, with 9.5 Coulombs of electrons dumped, occurred in January of 1982. Then the experiment was halted for the installation of 3 $m \times 3$ m detectors. The final run, with 20.4 Coulombs of electrons dumped, occurred in November and December of 1982.

At the beginning of the experiment, the experimental apparatus were checked using the "skyshines" produced in End Station A by inserting an 1/4" aluminum target into the electron beam. Timing of the fast electronics was also done with this arrangement. The beam position was checked by two remotely controlled ZnS screens, one in End Station A and one in front of Beam Dump East. After all these beam intercepting materials were withdrawn, the beam intensity would be increased to full blast to start data-taking. During a normal run, the beam intensity was typically $\sim 10^{14}$ electrons per second at a repetition rate of $\sim$ 170 pulses per second. With this beam intensity, the overall deadtime of the data acquisition system was less than $\sim$ 10%. Each experimental run lasted typically two to three hours. Then it was halted. The beam intensity was reduced and the repetition rate was dropped to $\sim$ 10 pulses per second to check the beam positions with ZnS roller screens. A new run would begin afterwards. During every 8-hours shift, a "skyshine" background run would be taken by inserting aluminum targets of various thickness (ranging from 1/16" to 1/2") into the beam at End Station A. Because of the high data rate under this condition, both intensity and pulse rate had to be reduced for these runs.

II.8 Experimental Backgrounds

The main background sources were cosmic rays and "skyshine". The cosmic ray backgrounds were mainly due to vertical air showers and could be accepted by the "energy threshold" trigger. The "skyshine" background was caused by pions which are produced by electrons interacting with residual

air in the beam pipe before the beam dump. Some of the pions thus produced would emerge into the air space above the top of the hill and interact with air to produce secondary pions, of which some would decay into muons in front of the detector to be accepted by the "horizontal muon" trigger.

It turned out that the running condition was quite clean. Beam associated "skyshine" background was investigated by inserting an 1/4" aluminum target into the beam at the End Station A to study the energy spectrum of the trigger from the muons. Since the hill subtended a small angle at the target, there were more pions emerging into the air above the hill. The trigger rate was approximately 3×10^6 per Coulomb of electron beam; it was dominated by the low energy muons triggers. The energy spectrum of the beam associated triggers is shown in Figure II.14. Most of the triggers were produced by particles of energies below 1 GeV. The trigger rate was less than 0.2 per Coulomb of electron beam with energy above 3 GeV. This is expected, because the muon is $\sim$ 200 times heavier than the electron and will radiate much less energy when traversing through material in the shower detector. Figure II.15 shows the time distribution of the triggers when the aluminum target was in the beam. The beam associated triggers were clearly seen above the general cosmic ray backgrounds. The width of the beam gate was set at 6 μsec. It was quite clear from the distribution that the triggers were beam associated within the 1.6 μsec beam spill time.

With the aluminum target removed triggers were dominated by cosmic rays with a rate of approximately 10^3 per Coulomb. The energy spectrum

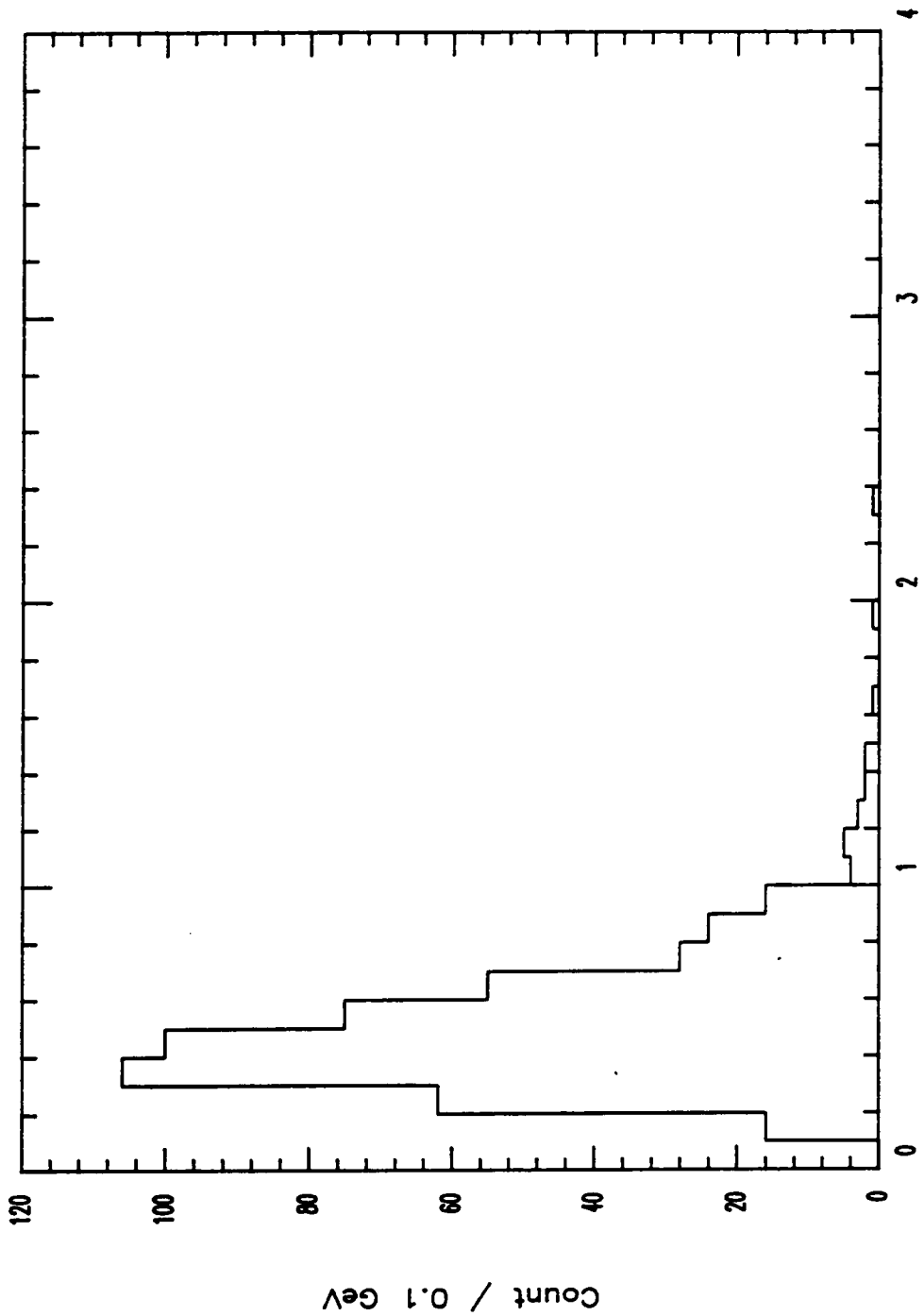

Figure II.14: Energy Spectrum of experimental triggers of beam associated skyshine with Al target in beam.

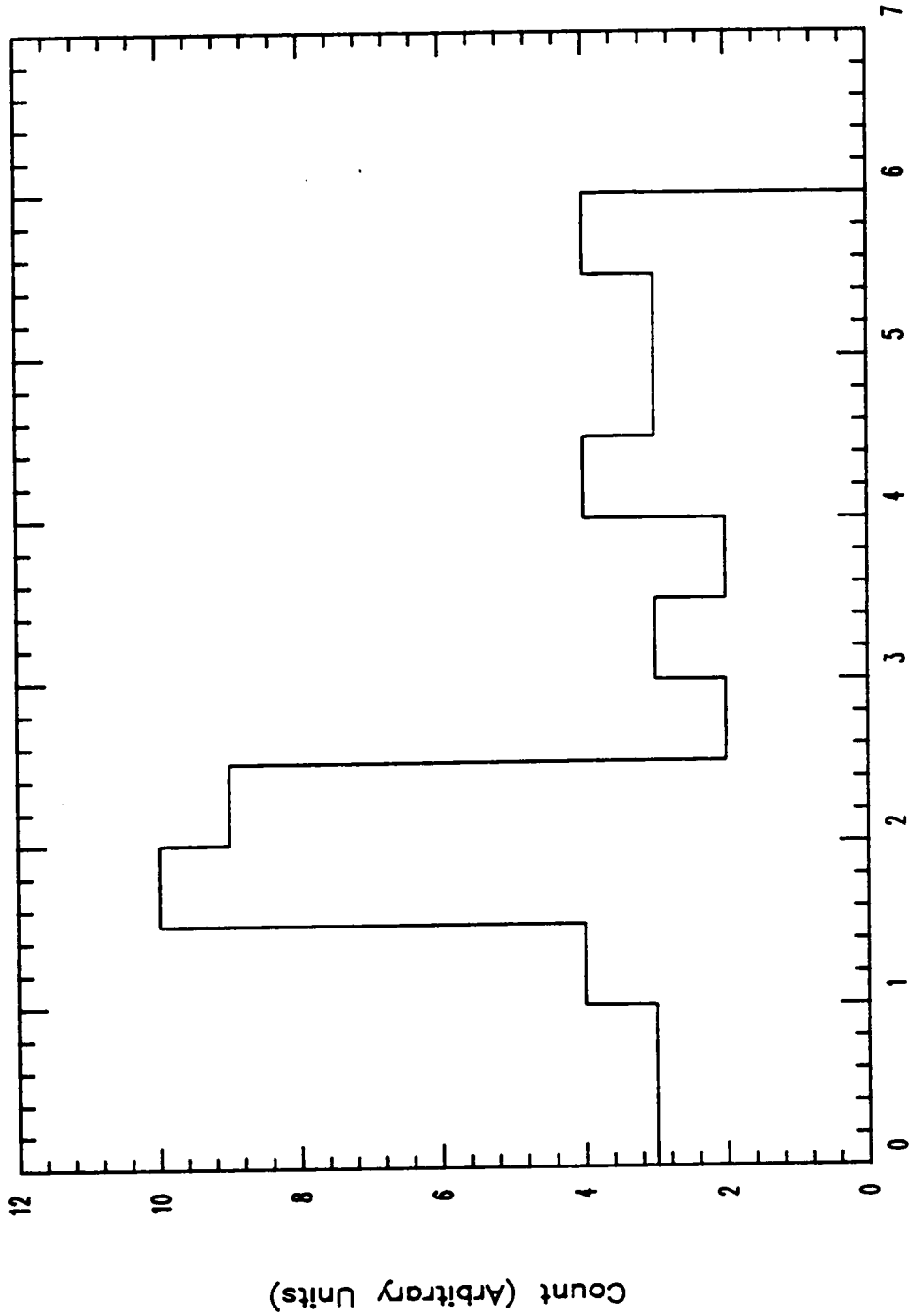

Figure II.15: Time distribution of the experimental triggers of the beam associated skyshine with removable Al target in beam.

is considerably harder as shown in Figure II.16. The angular distribution of the trigger is much broader, leading to easy rejection of almost all the triggers. Beam-associated signals were seen by examining the low energy component of the spectrum.

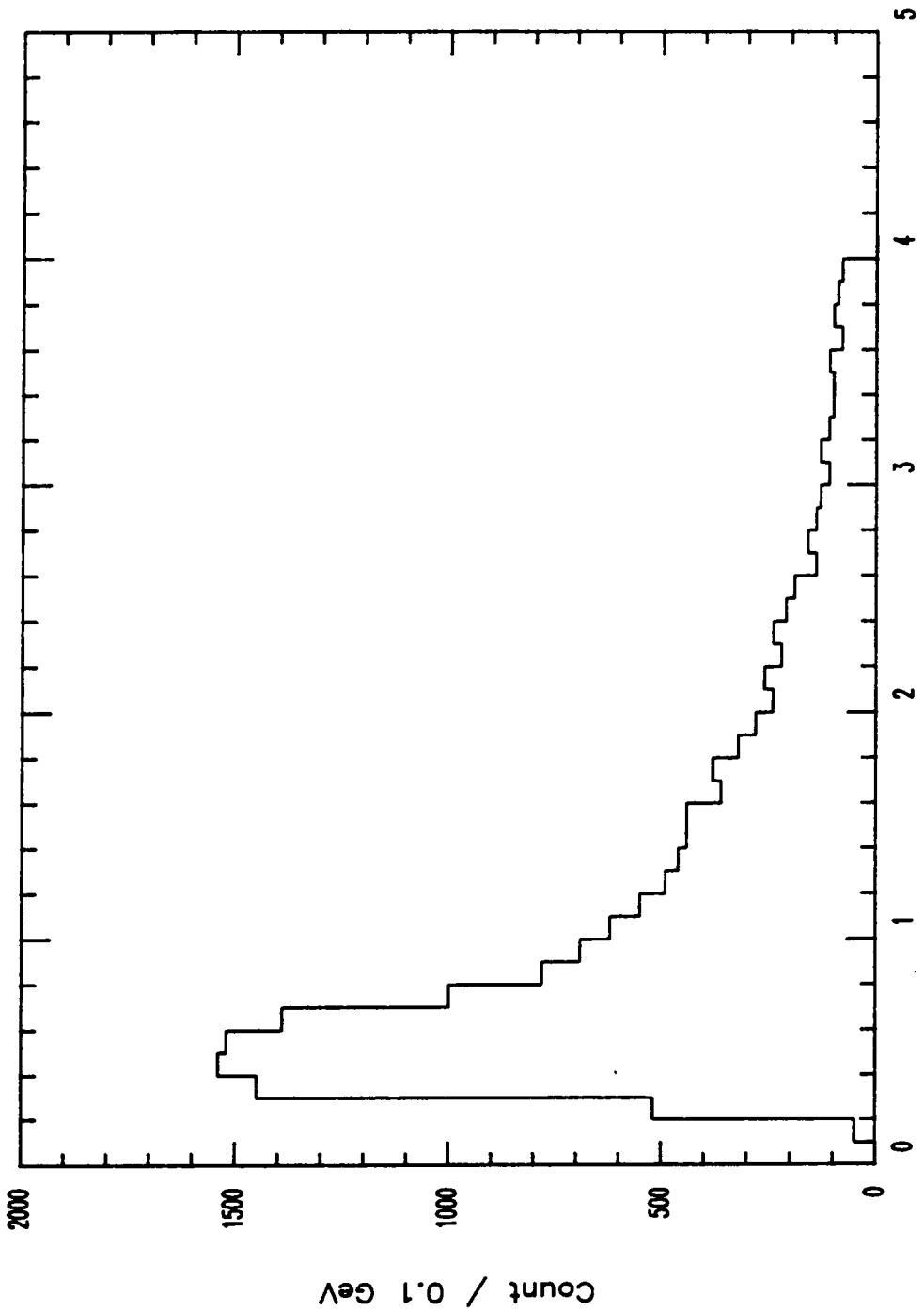

Figure II.16: Energy spectrum of the experimental triggers with Al target removed.

Chapter III

Data Analysis

By examining the experimental results as indicated by Figure II.14, it became evident that a minimum energy cut of 1 GeV was necessary to reject the triggers caused by the beam associated "skyshine" background. Since the hypothetical X particle beam was expected to be well collimated, the cosmic rays could be easily rejected by examining the angular distribution of the trigger and requiring the trigger to be in time with the beam. As the X particles might decay into electron-positron pairs or photons in flight, the candidates of interest would have the signature of a single or double showers pointing from the beam dump to the detector with very small angles.

After the final run the data were analyzed with the following procedure: Firstly, the data were processed with a very mild cut, only requiring that the data should be within the 2 μsec gate of the beam spill and that the energy should be greater than 1 GeV. This simple procedure immediately removed $\sim$ 75% of the data. For example, for the final 20.4 Coulombs run, out of $\sim$ 23,000 events recorded on magnetic tapes, only $\sim$ 6,000 of them survived the cut. The remaining triggers were then examined in great detail on a high

resolution graphics terminal (CGC 7900), together with other information such as total energy, timing, etc. The pulse height information from all the CCD's on one side of a chamber were combined together, and each display showed the x- or y- view of the combined pulse trains from all the chambers. Figure III.1 is a typical event display. From the display one could immediately see the track in each view as well as the shower development along the track. This enabled us to recognize immediately that the majority of these events were caused by either muons (which deposited an almost equal amount of energy in each layer of the chamber), or by cosmic ray showers (which had very large angles relative to the beam direction). After this computer-aided scan, where events which were observed to be grossly nondirectional were rejected, 189 events remained. The angles of these events were calculated by using the information from the MWPC's and after cuts, requiring vertical and horizontal angles less than 300 mr, 24 events remained. Only one event was found within a resonable fiducial region of horizontal angle less than 100 mr and vertical angle less than 30 mr, which were the approximate angles subtended by the earth shielding as seen by the detector. From the MWPC data alone, this surviving event could be regarded as a cosmic ray pointing toward the beam dump. But the trigger energy was less than 2 GeV which was too low for a cosmic ray shower. Combining the information from chambers and scintillation counter, this event could be understood as a muon radiating a photon in the front portion of the detector and then penetrating all layers of the detector. We thus ended up with no convincing candidate event.

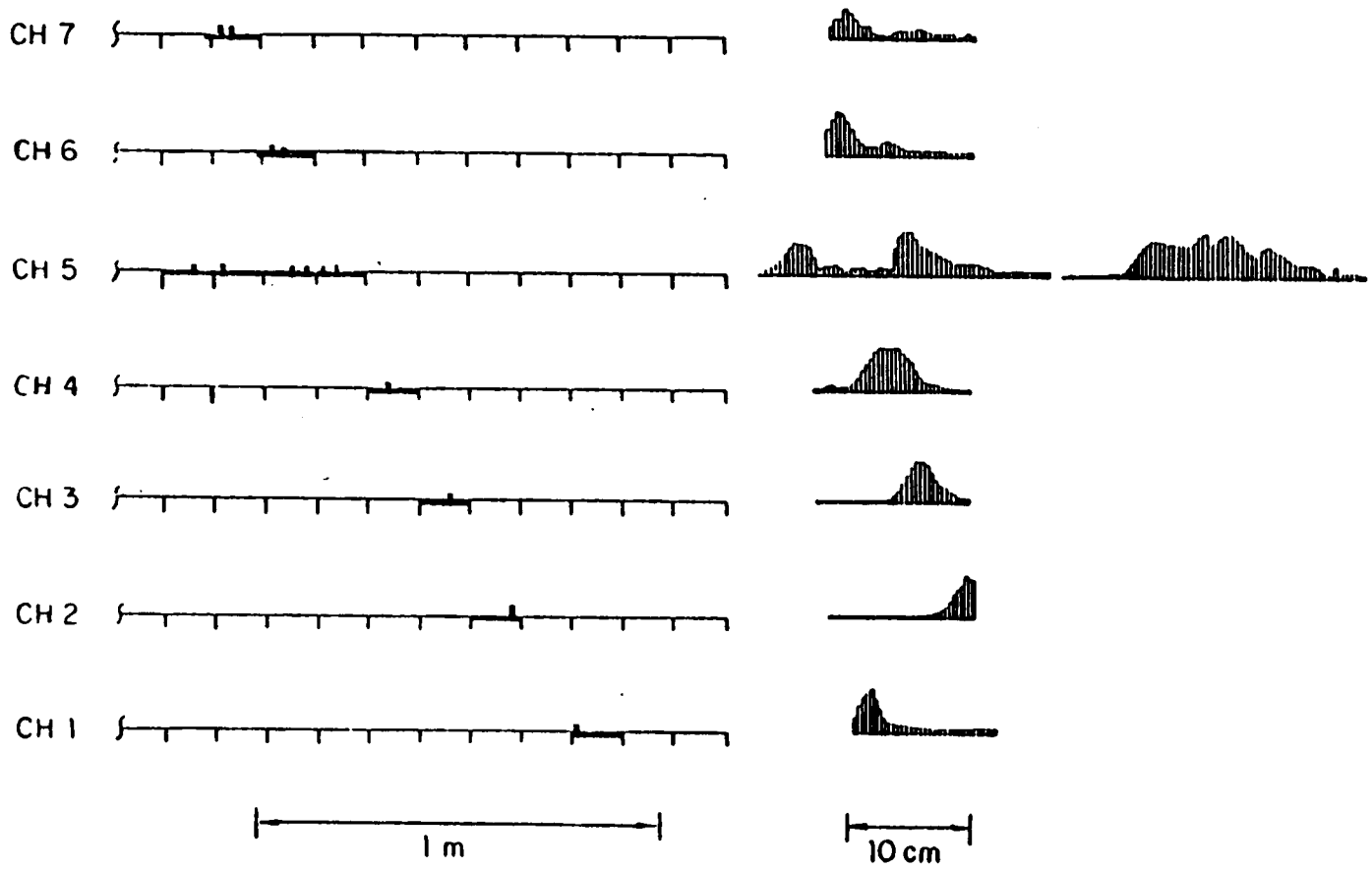

Figure III.1: An example of a typical event display on a graphics terminal during data analysis.

A second line of analysis was made to avoid the possible subjectivity associated with the computer-aided scanning. In this alternative analysis we raised the energy cut from 1 GeV to 3 GeV, requiring that the trigger be within the 2 μsec gate of the beam spill. To reject the large angle showers, we required that at least 2/3 of the energy be within a single row of scintillation counters. Only 36 events passed these criteria; and they overlapped the preceeding 189 events obtained from the computer-aided scan. Again this led to no candidate events.

For the earlier run with 9.6 Coulombs of 20 GeV electrons dumped, the detector was smaller, 2 m $\times$ 3 m, as described above. Using the same method of analysis for 5,586 triggers written on magnetic tapes, no candidate events were found.

Chapter IV

Discussion of Results

Although the axion-like particles and photinos were not found in the SLAC E137 experiment, the experimental results are useful in establishing limits. We will describe below how these limits were obtained.

IV.1 Axion-like Particles

In the SLAC E137 experiment, it was assumed that the axion-like particles could be produced by electrons, positrons and photons in the electromagnetic shower initiated by a primary 20 GeV electron beam interacting with water. They could be produced in the following four processes: the axion photo-production via the Primakoff effect[24], the electron or positron bremsstrahlung of axions[25], the axion resonance production in the annihilation of a high energy positron with an atomic electron, and the annihilation of a positron with an atomic electron into an axion and a photon. The production cross sections are given in Appendix B. The Feynman diagrams for these four processes are shown in Figure IV.1. It was also

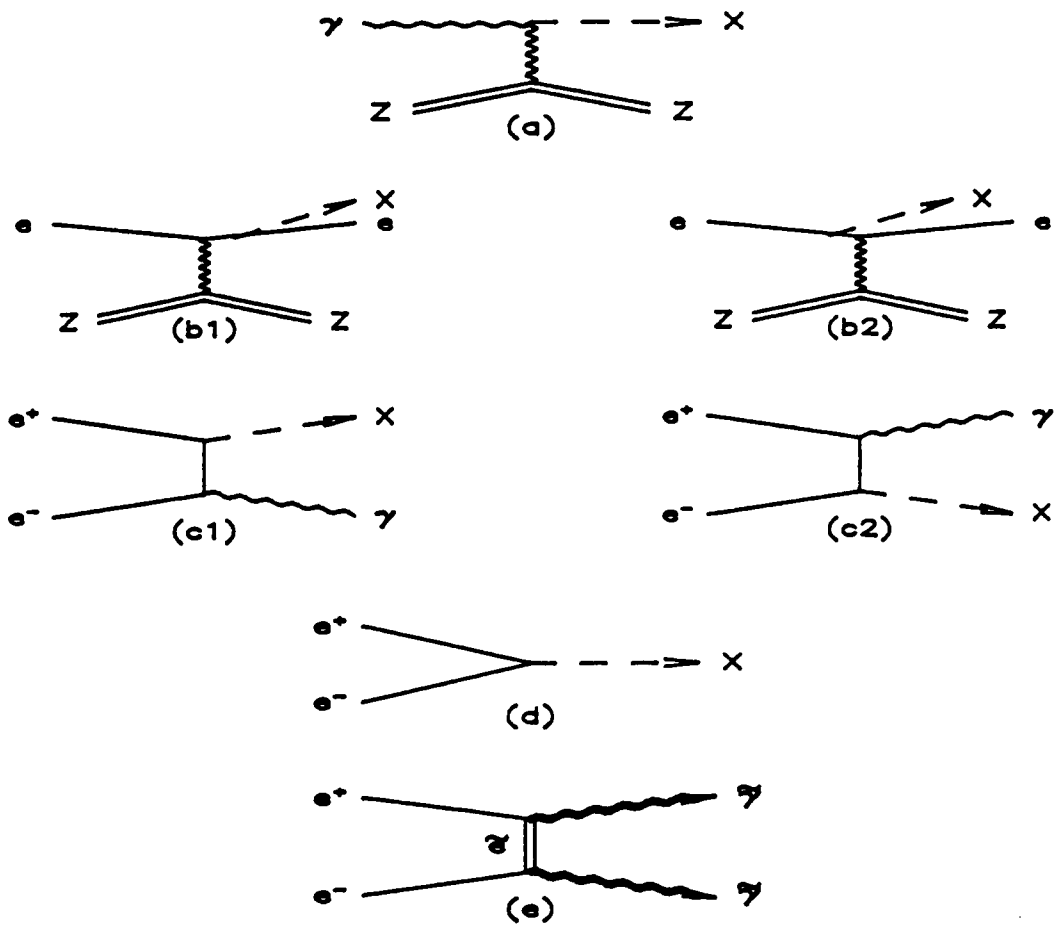

Figure IV.1: Feynman diagrams of the production process of the axions and photinos. (a) Photon-production of axions via the Primakoff effect. (b) Electron or positron bremsstrahlung of axions. (c) Annihilation of an electron-positron pair into an axion and a photon. (d) Resonance production of axions in the annihilation of an electron-positron pair. (e) Annihilation of an electron-positron pair into two photinos via selectron exchange.

assumed that the axion-like particle could decay into a pair of photons, or an electron-positron pair if its mass is heavier than twice the electron mass.

Since the decay of the axion is characterized by two parameters, F_X and m_X, all the axion production cross sections and decay rates are functions of F_X and m_X only. In addition, both the production cross section and decay rate are proportional to F_X^{-2}; hence the calculated detection rate of the axion is a function of F_X and m_X, and is proportional to F_X^{-4}. With 95% confidence level, the calculated rate should be less than or equal to 3 events, given that no axion was observed in this experiment. Figure IV.2 shows the lower limit on F_X obtained from this experiment for the axion decaying into two photons as a function of the axion mass. Figure IV.3 shows the lower limit on F_X for the axion decaying into an electron-positron pair as a function of the axion mass. The axion lifetime τ_X is proportional to F_X^2, and the lower limits on $m_X\tau_X$ are also obtained as functions of m_X, which are shown in Figures IV.4 and IV.5. Details of the calculations are given in Appendix A.

From the fact that the axion is a weakly coupled, penetrating, and neutral object, the interaction of the axion with material in the beam dump is neglected in the rate calculations. Also in calculating the rate, a threshold energy cut of 2 GeV was used. The expected energy spectrum of the axion is proportional to the track-length distribution of the shower particles in the beam dump. Figure IV.6 shows the track-length distribution of the photons. One can see that more than 50% of the expected axion flux with energy above 1 GeV actually lies above 2 GeV. Thus the rate, which is

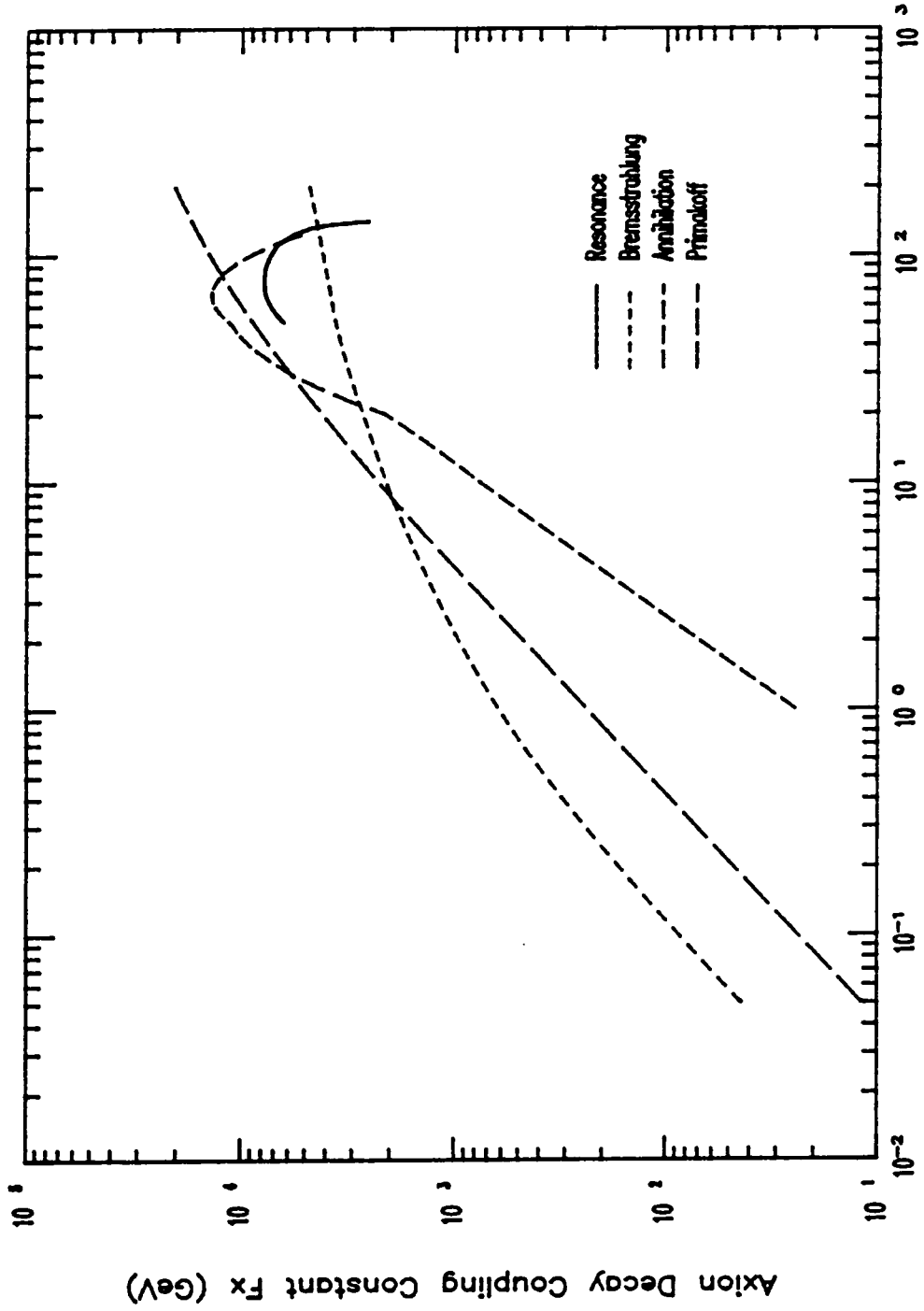

Figure IV.2: Lower limits on decay coupling constant F_X for the axion-like particle decay into two photons with 95% confidence level given by SLAC E137.

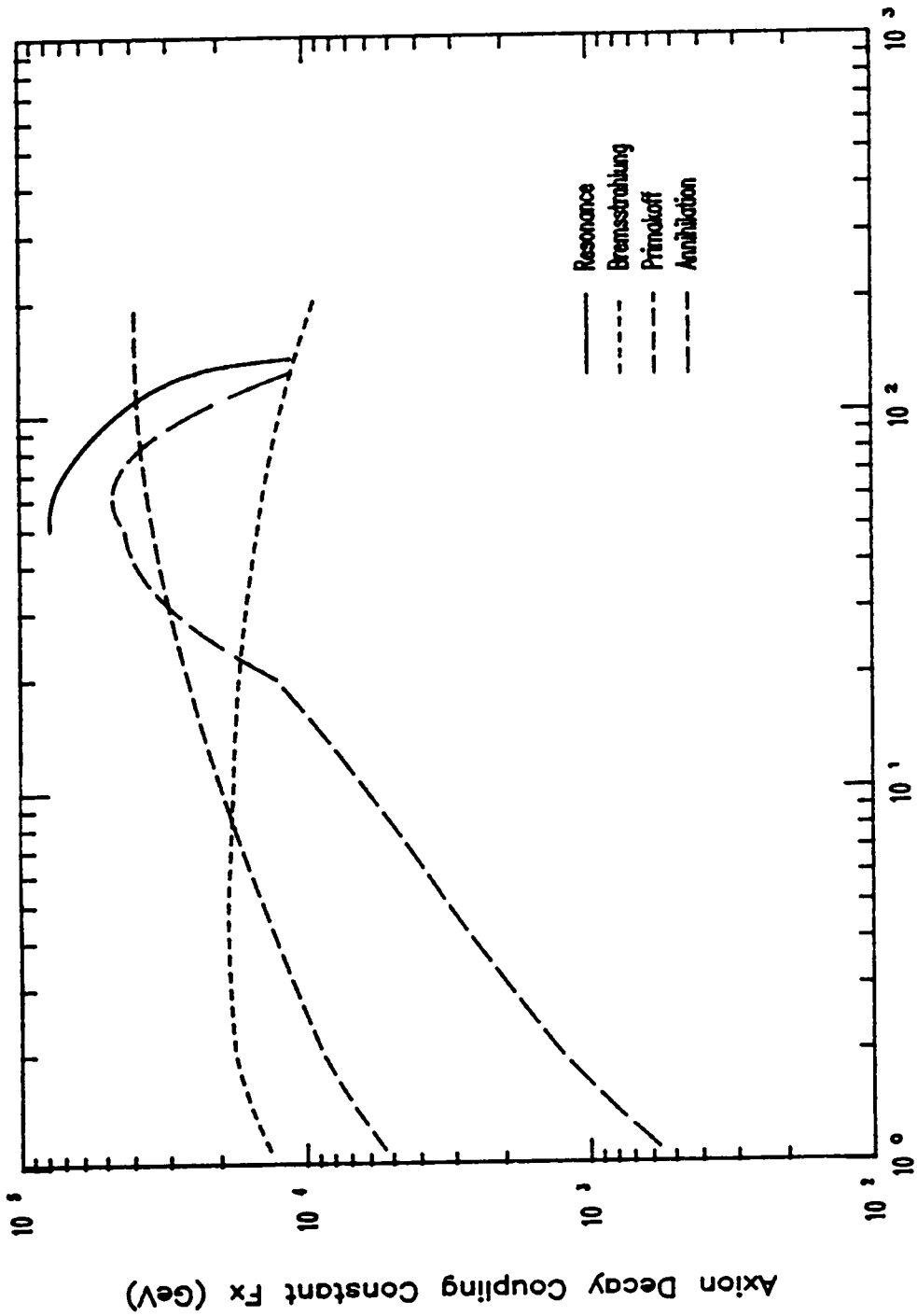

Figure IV.3: Lower limits on decay coupling constant F_X for the axion-like particle decay into an electron-positron pair with 95% confidence level given by SLAC E137.

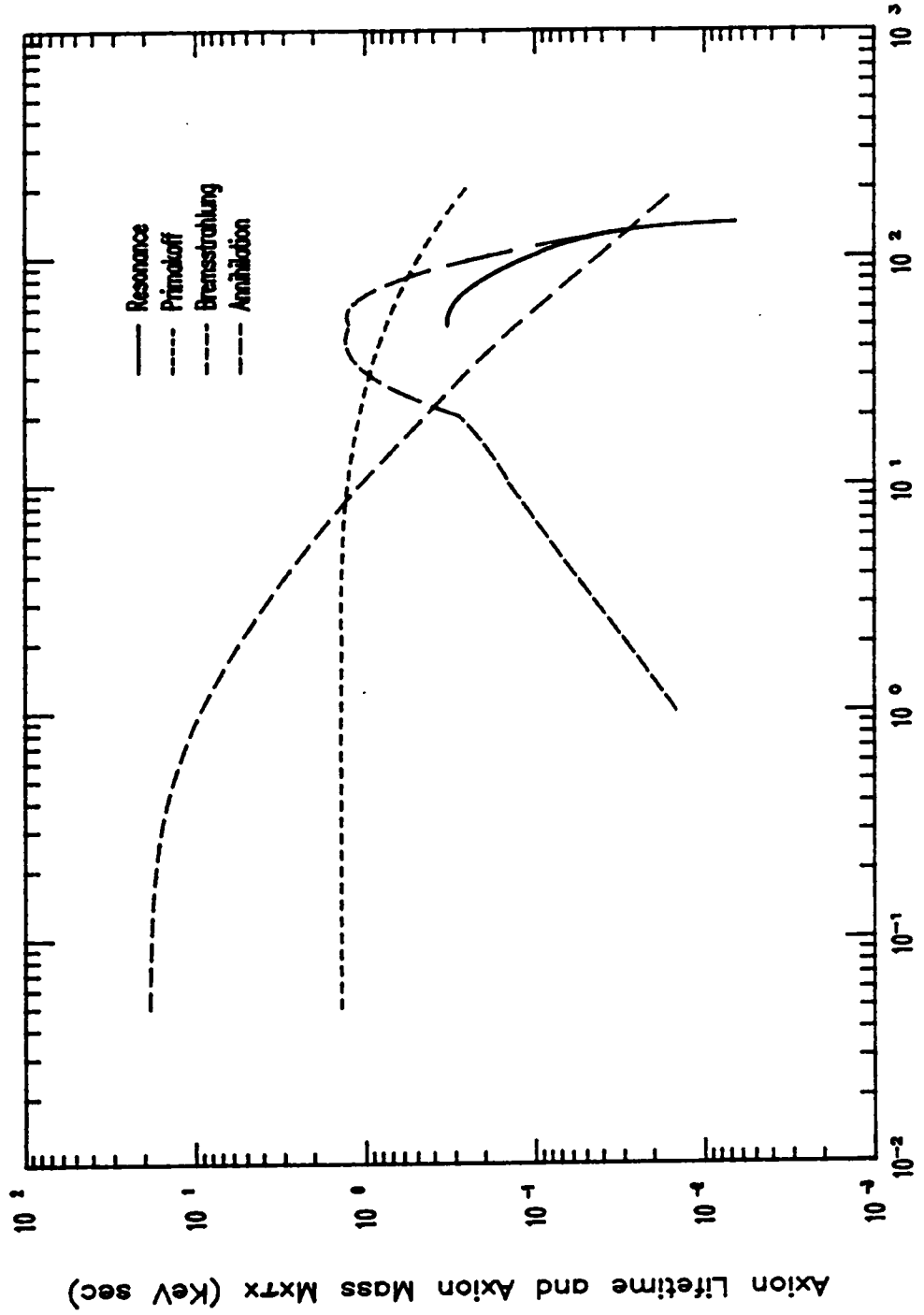

Figure IV.4: Lower limits on $\tau_X m_X$ for the axion-like particle decay into two photons with 95% confidence level given by SLAC E137.

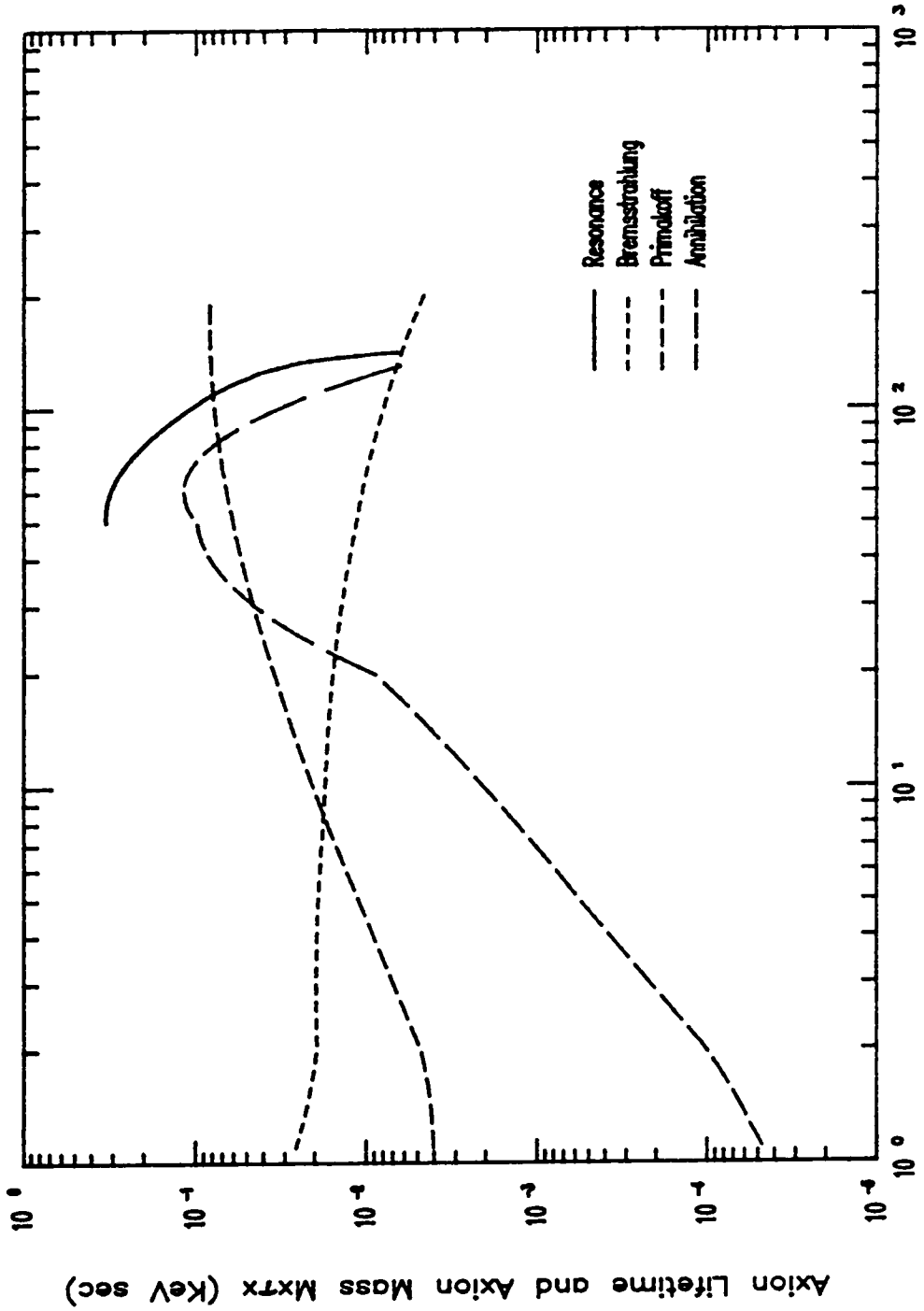

Figure IV.5: Lower limits on $\tau x m x$ for the axion-like particle decay into an electron-positron pair with 95% confidence level given by SLAC E137.

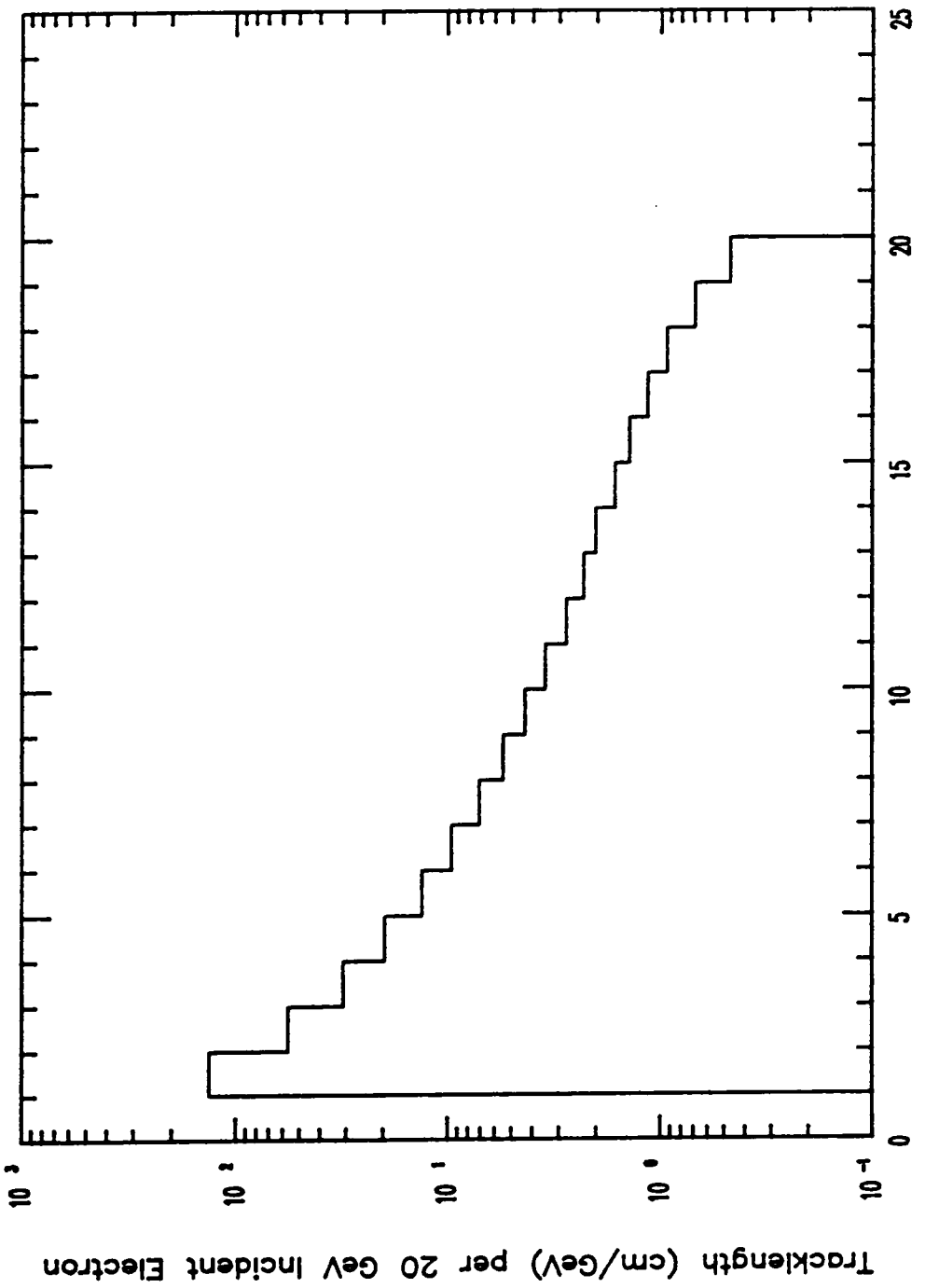

Figure IV.6: Distribution of the total photon tracklength of the electromagnetic shower initiated by a 20 GeV electron interacting with the water.

proportional to the tracklength, is not inordinately sensitive to the cut in energy.

As mentioned in the introduction, the axions we searched for are the generic axions. If the axion couples to the quarks, it could also be produced in a proton beam dump. In fact, the recent CERN proton beam dump experiment performed by the CHARM collaboration[28] covers the same region in the F_X - m_X space as this experiment did for the case of the axion decaying into two photons or an electron-positron pair. The CDHS experiment at CERN[27], in which the axion production mechanism was similar to that of CHARM, also covers the same region. The comparison of the three results in terms of the lower limit on the axion decay constant F_X in the axion mass range of 50 KeV/c^2 to 210 MeV/c^2 is given in Figure IV.7. An axion with mass greater than 1 MeV/c^2 will decay with bigger rate into an electron-positron pair than into two photons. Therefore, the lower limit of F_X set by the axion decaying into an electron-positron pair is much higher than that set by the axion decaying into two photons. Although the two CERN experiments give the similar lower limits on F_X to that of the SLAC E137 experiment, they cannot exclude the possibility if axions can only couple to electrons or photons. This experiment gives the first limit on F_X, for the case of axions which only couple to photons. This limit is shown in Figure IV.2 for the case in which the axion is produced by the Primakoff mechanism and decays into two photons.

The PQWW axion of mass in the 100 KeV/c^2 range was of interest a few years ago. The mass of the PQWW axion can be estimated to be

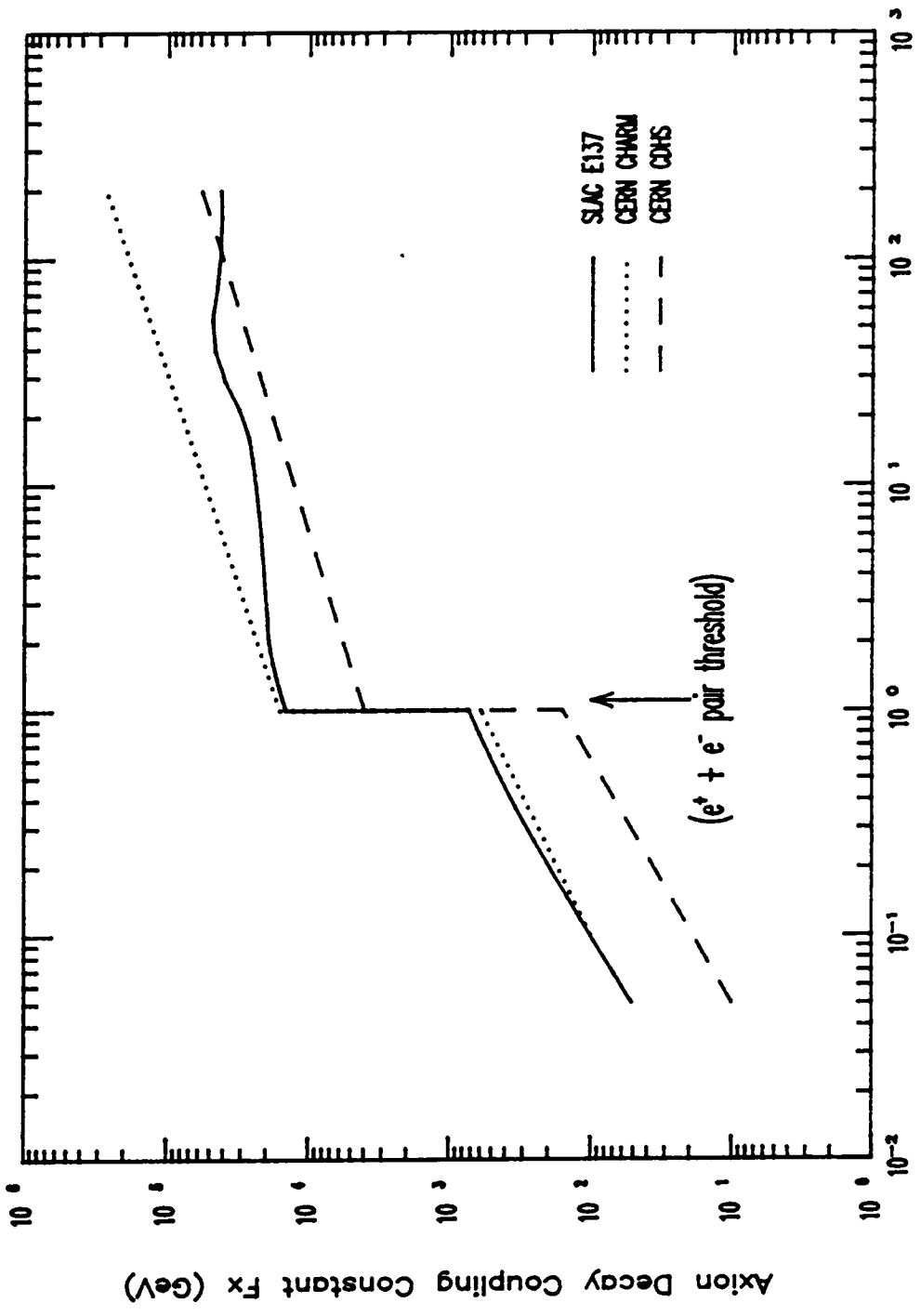

Figure IV.7: Lower limit on decay coupling constant F_X for axion-like particles with mass m_X less than 210 MeV (90% confidence level) given by SLAC E137, CERN CHARM and CERN CDHS.

$50N\ KeV/c^2$, where N is the number of quark families[7-9]. This kind of axion can only decay into two photons. One can relate the PQWW axion lifetime to that of the generic axion lifetime. Therefore, the limit we give here can also be translated into a limit for the classical axion. Details are given in Appendix B. Figure IV.8 shows the lower limit of the PQWW axion lifetime from this experiment. It can be seen that the sensitivity of this experiment to the light mass PQWW axion is somewhat marginal.

IV.2 Photino ($\tilde{\gamma}$)

A pair of photinos could be produced in positron annihilation with an atomic electron via exchange of a selectron [36] as shown in Figure IV.1. The positrons were those in the electromagnetic shower initiated by 20 GeV electron beam in water. The photino could decay into a massless goldstino and a photon. Only the photon can be detected. Experiment E137 is the first one that proposed the search for light mass photinos. Its production cross section is lower than that for the e^+e^- colliders by a factor of $\sim 10^6$. However, the luminosity for this fixed target experiment is higher than that for the e^+e^- colliders by also a factor of $\sim 10^6$; therefore, this beam dump experiment is very competitive.

The photino production cross section and decay probability depend on a few unknown parameters which are the photino mass, selectron mass, and the supersymmetry breaking scale, $d^{1/2}$. Our experimental results can provide a lower limit on the parameter, $d^{1/2}$, as a function of photino mass, parametrized by the selectron mass, as shown in Figure IV.9. Details of

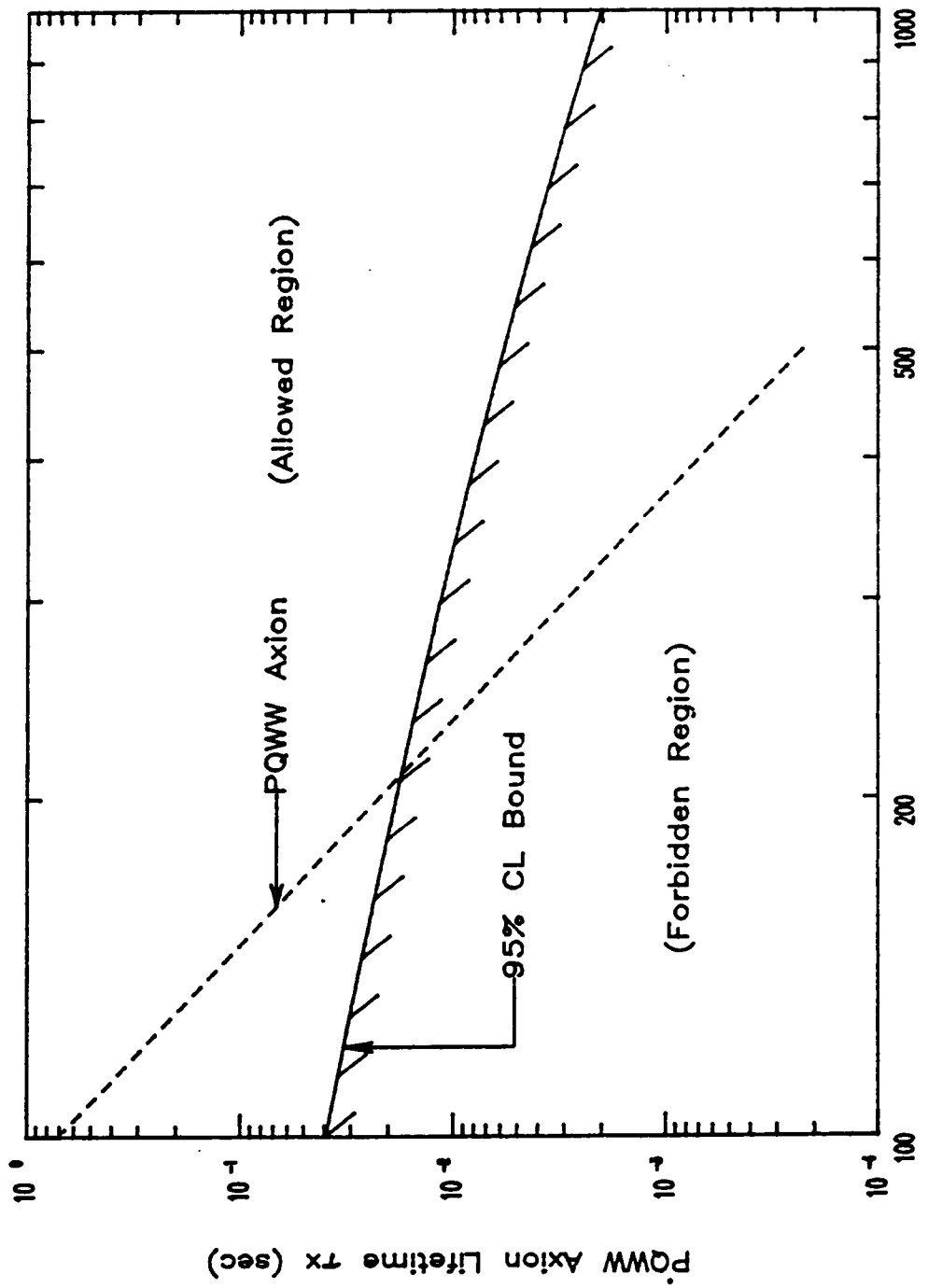

Figure IV.8: Lower limit on PQWW axion lifetime τ_X with 95% confidence level given by SLAC E137.

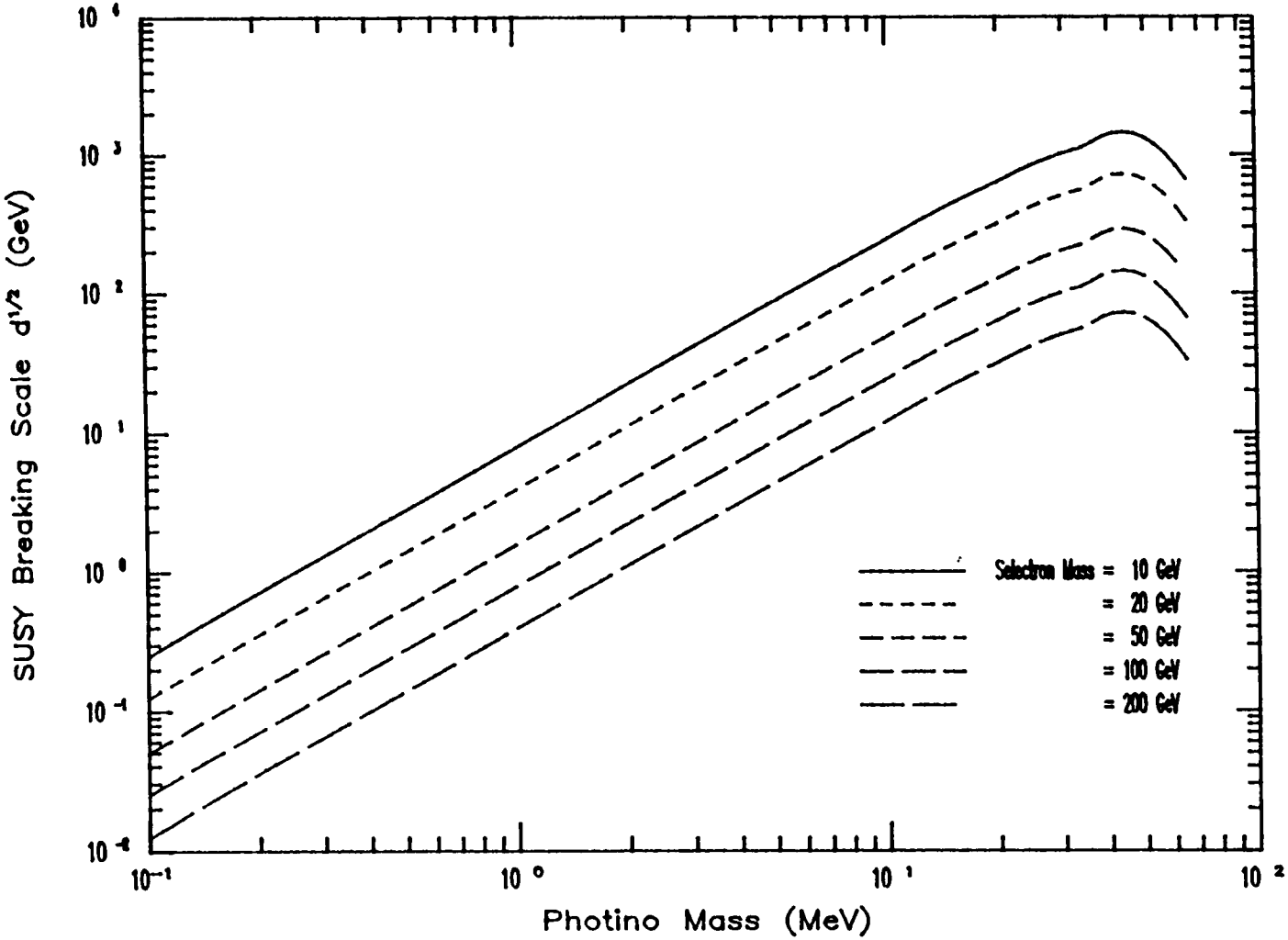

Figure IV.9: Lower limits on the supersymmetry breaking scale $d^{1/2}$ for the photino decay into a photon and a goldstino with 95% confidence level given by SLAC E137.

the calculation is given in Appendix A.

References

[1] J. R. Kilmer, L. W. Mo, T. A. Nunamaker, R. Orr, and T. E. Toohig, Fermilab Experiment Proposal P635

[2] P. Fayet and S. Ferrara, Phys. Rep. 32*C*, 249(1977)

[3] H. Fritzsch, M. Gell-Mann, and H. Leutwyler, Phys. Lett. 47B, 365(1972); D. J. Gross, and F. Wilczek, Phys. Rev. D 8, 3497(1973); S. Weinberg, Phys. Rev. Lett. 31, 494(1973)

[4] F. E. Close, An Introduction to Quarks and Partons (Academic Press, New York, 1979).

[5] A. A. Belavin, A. M. Polyakov, A. S. Schwartz, and Yu. S. Tyupkin, Phys. Lett. 59B, 85(1978); G. t'Hooft, Phys. Rev. D 14, 3432(1976)

[6] P. Ageron, C. A. Baker, S. A. Clark, K. Green, B. Heckel, A. I. Kilvington, W. Mampe, P. C. Miranda, J. Morse, J. M. Pendleburg, N. F. Ramsey, K. F. Smith, R. Golub, J. Byrne, T. J. L. McComb, T. J. Sumner, S. M. Burnett, and A. R. Taylor, Phys. Lett. 136B, 327(1984)

[7] R. D. Peccei and H. R. Quinn, Phys. Rev. Lett. 38, 1440(1977); Phys. Rev. D 16, 1791(1977)

[8] F. Wilczek, Phys. Rev. Lett. 40, 279(1978)

[9] S. Weinberg, Phys. Rev. Lett. 40, 223(1978)

[10] C. N. Yang, and R. L. Mills, Phys. Rev. 96, 191(1954)

[11] S. Weinberg, Phys. Rev. Lett. 19, 1264(1967); A. Salam, Elementary Particle Physics, ed. N. Svartholm (Almquist and Wiksells, Stockholm, 1968)

[12] T. W. Donnelly, S. J. Freedman, R. S. Lytel, R. D. Peccei, and M. Schwartz, Phys. Rev. D 18, 1607(1978)

[13] D. Antreasyan, D. Aschman, E. Bloom, F. Bulos, T. Burnett, M. Cavalli-Sforza, R. Chestnut, D. Coyne, J. Gaiser, D. Gelphman, G. Godfrey, Y. F. Gu, R. Hofstadter, R. Horisberger, C. Kiesling, I. Kirkbride, H. Kolanoski, W. Kollmann, K. Kõnigsmann, R. Lee, W. Lockman, C. Newman, M. Oreglia, M. Richardson, H. F. W. Sadrozinski, D. L. Scharre, K. Strauch, K. Wacker, and A. Weinstein, Phys. Rev. Lett. 48, 903(1982)

[14] G. Blanar, T. Böhringer, H. Dietl, G. Eigen, P. Franzini, K. Han, S. W. Herb, J. E. Horstkotte, R. Imlay, C. Klopfenstein, J. Lee-Franzini, G. Levman, E. Lorenz, G. Mageras, W. Metcalf, F. Pauss, D. Peterson, E. Rice, R. D. Schamberger, Jr., M. Sivertz, L. J. Spencer, V. Sreedhar, P. M. Tuts, H. Vogel, and J. K. Yoh, Phys. Rev. D 26, 717(1982)

[15] M. Alam, D. Andrews, P. Avery, C. Bebek, K. Berkelman, D. G. Cassel, A. Chen, K. Chadwick, J. Chauveau, S. E. Csorna, J. W. Dewire, R. Ehrlich, T. Ferguson, A. Fridman, R. Galik, P. Ganci, L. Garren, T. Gentile, M. G. D. Gilchriese, B. Gittelman, M. Goldberg, J. Green,

Joan A. Guida, A. M. Halling, D. L. Hartill, J. Hassard, M. Hempstead, D. Herrup, R. Hicks, S. Holzner, N. Horwitz, M. Ito, J. M. Izen, A. Jawahery, M. Jibaly, P. Lipari, H. Kagan, J. Kandaswamy, K. Kinoshita, R. Kass, V. Kistiakowsky, D. L. Kreinick, Y. Kubota, W. W. MacKay, A. C. Melissinos, M. D. Mestayer, N. B. Mistry, G. C. Moneti, F. Morrow, E. Nordberg, M. Ogg, S. L. Olsen, G. Parkhurst, R. S. Panvini, R. Perchonok, F. M. Pipkin, R. Plunkett, R. Poling, J. Rohlf, C. Rosenfeld, G. Rucinski, A. J. Sadoff, F. Sannes, A. Silverman, P. Skubic, A. Snyder, P. C. Stein, R. Stone, S. Stone, E. H. Thorndike, G. Tranhern, H. Van Hecke, D. Weber, R. Wilcke, and Richard Wilson, Phys. Rev. D 27, 1665(1983)

[16] G. Alexander, A. Av-Shalom, G. Bella, J. K. Bienlein, K. W. Chen, M. Coles, A. Engler, G. Floger, A. Fridman, R. Graumannm, J. Grunhaus, F. H. Heimlich, Z. Jakubowski, A. C. Kõnig, R. W. Kraener, W. Langguth, B. Lurz, D. Marlow, F. Messing, R. Nernst, B. Niczyporuk, C. Rippich, M. Scheer, M. Schmitz, D. J. Schotanus, A. Schwarz, U. Strohbusch, H.-J. Trost, H. Vogel, U. Volland, H. Wegener, S. Youssef, T. Zeludziewicz, and P. Zschorsch, Z. Physik C17, 197(1983)

[17] F. Boehm, F. V. Feilitzsch, A. A. Hahn, H. Kwon, R. L. Mõssbauer, and J. Vuilleumier, Phys. Lett. 101B, 341(1982)

[18] F. P. Calaprice R. W. Dunford, A. Hallin, R. T. Kouzes, M. Miller, M. Schneider, and D. Schreiber, Phys. Rev. D 20, 2708(1979)

[19] A. Zehnder, Phys. Lett. 104B, 494(1981)

[20] D. J. Bechis, T. W. Dombeck, R. W. Ellsworth, E. V. Sager, P. H. Steinberg, L. J. Tieg, R. L. Weitz, and J. K. Yoh, Phys. Rev. Lett. 42, 1511(1979)

[21] R. L. Burman, D. R. F. Cochran, J. Duclos, J. S. Frank, C. K. Hargrove, V. W. Hughes, H. Kaspar, U. Moser, P. Nemethy, R. P. Redwine, and S. E. Willis, Phys. Rev. D 28, 1790(1983)

[22] F. Reines, H. S. Gurr, and H. W. Sobel, Phys. Rev. Lett. 37, 315(1976)

[23] J. D. Bjorken, Search for Neutral Penetrating, Metastable Particles in the SLAC Beam Dump, Rencontre de Moriond (1984) p227

[24] A. Halprin, C. M. Anderson, and H. Primakoff, Phys. Rev. 152, 1295(1966)

[25] Y. S. Tsai, Phys. Rev. D 34, 1326(1986)

[26] A. Abashian, J. D. Bjorken, L. W. Mo, W. R. Nelson, and Y. S. Tsai, SLAC Experimental Proposal (E137)

[27] P. Debu, private comminucation

[28] I. Abt, J. V. Allaby, U. Amaldi, J. Aspiazu, G. Barbiellini, A. Baroncelli, L. Barone, C. Berger, F. Bergsma, B. Borgia, C. Bosio, F. W. Büsser, A. Capone, H. Daumann, M. Diemoz, U. Dore, J. Dorenbosch, F. Ferroni, W. Flegel, P. D. Gall, P. Gorbunov, E. Grigoriev, T. Herbbeker, V. Kaftanov, V. Khovansky, L. Lanceri, E. Longo, L.

Luminari, M. Metcalf, P. Monacelli, F. Niebergall, C. Nieuwenhuis, F. De Notaristefani, J. Panman, P. Pistilli, A. Rosanov, R. Santacesaria, C. Santoni, P. Schütt, P. Stähelin, L. Tortora, V. Valente, and K. Winter, Phys. Lett. 157B, 458(1985)

[29] J. Badier, C. Bemporad, J. Boucrot, O. Callot, P. Chapentier, A. M. Cnops, M. Crozon, P. Delpierre, J. F. Detoeuf, G. R. Giannini, R. Hammarstrom, P. Lariccia, R. Lorenzi, J. Mas, A. Michelini, A. Tilquin, and J. K. Walker, Z. Phys. C31, 21(1986)

[30] R. D. Peccei, T. T. Wu, and T. Yanagida, Phys. Lett. 172B, 435(1986); L. M. Krauss and F. Wilczek, Phys. Lett. 173B, 189(1986)

[31] P. de Barbaro et al. (to be published)

[32] M. Davier, J. Jeanjean and H. Nguyen Ngoc, Phys. Lett. 180B, 295(1986)

[33] A. Enomoto, Y. Fukushima, K. Imai, E. Kikutani, H. Koiso, A. Konaka, H. Kobayashi, A. Masaike, H. Matsumoto, K. Miyake, K. Nakahara, T. Nakamura, N. Nagamine, S. Ohsawa, N. Sasao, I. Sato, T. Taniguchi, and Urakawa, Phys. Rev. Lett. 57, 659(1986)

[34] M. R. Adams, C. N. Brown, W. E. Cooper, J. A. Crittenden, D. A. Finley, H. D. Glass, R. Gray, Y. Hemmi, Y. B. Hsiung, J. R. Hubbard, K. Imai, D. E. Jaffe, A. M. Jonckheere, H. Jostlein, D. M. Kaplan, L. M. Lederman, K. B. Luk, A. Maki, Ph. Mangeot, R. L. McCarthy, K. Miyake, R. E. Plagg, J. P. Rutherfoord, Y. Sakai, N. Sasao, S. R.

Smith, P. B. Straub, N. Tamura, T. Yoshida, and K. K. Young, Phys. Rev. Lett. 57, 2101(1986)

[35] N. Cabibbo, G. R. Farrar and L. Maiani, Phys. Lett. 105B, 155(1981)

[36] J. Ellis, and J. S. Hagelin, Phys. Lett. 122B, 303(1983)

[37] G. D'Agostini, R. Aleksan, W.-D. Apel, S. Banerjee, H.-J. Behrend, J. Bodenkamp, W. De Boer, G. Buschhorn, Bouchez, G. Carnesecchi, Ch. Chen, P. Colas, A. Cordier, G. Cozzika, M. Davier, Y. Ducros, J. Engler, H. Fenner, J. H. Field, G. Flügge, D. Fournier, D. C. Fries, W. Fues, A. Gaidot, K. Gamerdinger, R. George, M. Goldberg, Grindhammer, J. F. Grivaz, P. Grosse-Weismann, B. Grossetete, U. Gümpel, B. Gunderson, Haissinski, O. Hamon, G. Hopp, V. Journe, F. Kapusta, F. Kovacs, C. Kiesling, A. Klarsfeld, R. Kotthaus, U. Kruse, H. Kuster, F. Laplanche, Y. Lavagne, H. Lierl, G. London, D. Lüers, U. Mallik, H. Müller, H. Oberlack, J. Pamela, J. P. Pansart, F. Pierre, L. Poggioli, H. Ramdoll, M. Rivoal, P. Schacht, M.-J. Schachter, G. Schmidt, H. Schneider, V. Schröder, H. Sindt, and J.-J. Veillet, Phys. Lett. 123B, 127(1983)

[38] J. Allison, K. Ambrus, J. Baines, A. H. Ball, R. J. Barlow, W. Bartel, L. Becker, S. Bethke, J. Chrin, D. Clarke, D. Cords, A. Dieckmann, G. Dietrich, C. Dowdery, I. P. Duerdoth, E. Elsen, R. Felst, A. Finch, F. Foster, R. G. Glasser, D. Haidt, J. Heintze, G. Heinzelmann, K. H. Hellenbrand, R. D. Heuer, G. Hughes, J. Huttunen, H.

Junge, H. Kado, J. Kanzaki, T. Kawamoto, G. Knies, T. Kobayashi, S. Komamya, M. Koshiba, H. Krehbiel, J. von Krogh, P. Laurikainen, P. Lennert, F. K. Loebinger, A. A. Macbeth, R. Marshall, H. Matsumura, K. Meier, R. Meinke, H. E. Mills, M. Minowa, P. G. Murphy, B. Naroska, M. Nozaki, T. Nozaki, J. Nye, S. Odaka, J. Olsson, S. Orito, G. F. Pearce, A. Petersen, E. Pietarinen, H. Rieseberg, S. Sato, D. Schmidt, U. Schneekloth, J. A. J. Skard, J. Spitzer, P. Steffen, K. Stephens, H. Takeda, T. Takeshita, Y. Tosuka, A. Wagner, S. R. Wagner, P. Warming, G. Weber, J. B. Whittaker, S. Yamada, M. Zachara, G. T. Zorn, Phys. Lett. 139B, 327(1984)

[39] B. Adeva, D. P. Barber, U. Becker, J. Burdugo, A. Bohm, J. G. Branson. J. D. Burger, M. Capell, M. Cerrada, H. S. Chen, M. Chen, M. L. Chen, M. Y. Chen, Y. S. Chu, R. Clare, E. Deffur, M. Demarteau, P. Duinker, H. S. Fesefeldt, D. Fong, M. Fukushima, R. D. Han, D. Harting, T. Hebbeker, G. Herten, M. C. Ho, M. Hussain, M. M. Ilyas, D. Z. Jiand, W. Krenz, P. Kuijer, Q. Z. Li, D. Luchey, E. J. Luit, C. Mana, M. A. Marquina, G. G. G. Massro, R. Mount, K. Nadeem, H. Newman, M. Pohl, F. P. Poschmann, R. R. Rau, S. Rodriguez, M. Rohde, J. A. Rubio, H. Rykaczewski, J. Salicio, I. Schultz, H. Stone, G. M. Swider, H. W. Tang, D. Teuchert, Samuel C. C. Ting, K. L tung, M. Q. Wang, M. White, H. G. Wu, S. X. Wu, B. Wyslouch, B. X. Yang, C. C. Chang, B. Zhou, R. Y. Zhu, and Y. C. Zhu, Phys. Rep. 109, 131(1984)

[40] M. Althoff, G. Baranko, F. Barreiro, K. W. Bell, R. Beuselinck, D. M. Binnie, M. G. Bowler, S. Brandt, W. Braunschweig, P. Bull, A. Caldwell, R. J. Cashmore, M. Cherney, P. E. L. Clarke, P. Dauncey, R. Devenish, M. Dittmar, P. J. Dornan, E. Duchovni, Y. Eisenberg, J. Eisenmann, A. Eskreys, H. M. Fischer, B. Foster, G. E. Forden, R. Forhmann, D. A. Garbutt, G. Gather, P. Grossmann, J. C. Hart, H. Hartmann, J. Harvey, D. K. Hasell, C. M. Hawkes, E. Hillger, H. Holanoski, M. Holder, H. Hultschig, J. M. Izen, A. Jacksch, C. Jenkins, T. D. Jones, W. G. Jones, P. Joose, U. Karshon, F. J. Kirschfink, G. Knop, U. Kötz, H. Kowalsky, T. Kracht, H. L. Krasemann, G. Kreutz, H. Kuck, A. Ladage, P. Leu, S. L. Lloyd, B. Lohr, E. Lohrmann, K. Lübelsmeyer, D. Luke, H.-U. Martyn, P. Mättig, J. McCardle, D. J. Mellor, M. Mermikides, V. Mertens, G. Mikenberg, R. Mir, B. Neumann, D. Notz, R. J. Nowak, D. Pandoulas, G. Poelz, K. U. Pösnecker, J. Pyrlik, D. Revel, S. Ritz, E. Ronat, R. Rosskamp, G. Rudolph, M. Rushton, D. H. Saxon, D. Schmitz, W. Schütte, J. K. Sedgbeer, A. Shapira, H. Siebke, D. Strom, M. Takashima, J. Thomas, D. Trines, T. Tymieniecka, H. Venkataramania, W. Wallraff, W. A. T. Wan Abdullah, R. Wedemeyer, E. Wicklund, B. H. Wiik, M. Winik, G. Wolf, Sau Lan Wu, Ch. Xiao, G. Yekutieli, C. Youngman, and Zobernig, Z. Physik C26, 337(1984)

[41] Collaboration members are:

J. D. Bjorken (Fermilab, Batavia, Il 60510), S. Ecklund and W. R.

Nelson (SLAC, Standford, CA 94305), A. Abashian, C. Church, B. Lu, L. W. Mo, T. Nunamaker and P. Rassmann (Physics Department, Virginia Polytechnic Institute and State University, Blacksburg, VA 24061)

[42] H. S. Butler, S. K. Howry and C. H. Moore, SLAC Report 29 (1964)

[43] D. A. G. Neet, SLAC Report 68 (1966)

[44] A. Abashian, N. E. Booth,, C. C. Chang, R. H. Heisterberg, K. A. Lefler, C. Li, L. W. Mo, T. A. Numaker, A. Skuja, and H. Wang, Phys. Rev. Lett. 44, 635(1980)

[45] T. A. Nunamaker, R. Heisterberg, and L. W. Mo, Nclu. Inst. Meth. 175, 331(1980)

[46] W. R. Nelson, H. Hirayama and D. Rogers, SLAC Report 265 (198?)

[47] K. J. Kim, and Y. S. Tsai, Phys. Rev. D 8, 3109(1973); Y. S. Tsai, Rev. Mod. Phys. 46, 815(1974)

[48] R. Hofstadter, Electron Scattering and Nuclear Structure, a Collection of Reprints with an Instruction (W. A. Benjamin, New York, 1963).

[49] S. L. Glashow, and S. Weinberg, Phys. Rev. Lett. 20, 224(1968); R. Dashen, Phys. Rev. 183, 1245(1969)

Appendix A

Calculations of Event Rates

The event rate calculations for experiment E137 were handled by a Monte-Carlo program. The procedure is described in the following.

After the 20 GeV primary electron beam from the accelerator reached Beam Dump East, it interacted with water contained in the aluminum vessel producing electromagnetic showers. The shower particles would interact with water again, producing axions and photinos. The axions and photinos would be detected if they decayed in the air space in front of the detector. The program took the tracklength distribution of the shower particle as the input to calculate the axion production spectra. Then, it followed each axion (with given energy and direction) to the axion decay vertex position, and then weighted the axion event with the production and detection efficiency at that particular location. The total detection rate was obtained by summing up the results for all the axion production energies and directions.

For simplicity, we describe here only the calculations for the second experimental run with the 3 m $\times$ 3 m detector. The 3 m $\times$ 3 m detector was described in the computer program as a mosaic of 144 small pieces.

Each piece of the mosaic has a dimension of 25 cm × 25 cm, which is much larger than the spatial resolution of the detector ($\sim$ 3.6 mm). For the case of 2 m × 3 m detector used in the first experimental run, the same analysis program was used but with a different mesh.

The energy distribution of an electromagnetic shower can be described by its tracklength. The tracklength per unit energy is defined as

$$\frac{dL}{dE} = \int_0^\infty dt\pi(E,t), \tag{A.1}$$

where $\pi(E,t)$ is the average number of shower particles with energy between E and $E+dE$ at depth t in the dump. The tracklength distributions of photons, electrons and positrons were calculated by utilizing a Monte-Carlo program, EGS, developed at SLAC[46]. This program is designed to simulate electromagnetic showers in various geometries and at different energies. In this case, the particles were produced by the 20 GeV electron beam interacting with water in the Beam Dump East. From symmetry consideration, only the distributions of those shower particles aimed at the 36 mosaics of the first quadrant of the detector were computed. It turned out that 33% of photon tracklength, 23% of the electron tracklength, and 11% of positron tracklength were aimed at the 50 cm × 50 cm area, consisting of four "small" detectors, at the center of the detector. The minimum energy cut was 1 GeV. The tracklength distribution for each "small" detector was calculated separately, and was sliced into 1 GeV bins. The shower particles within a ΔE bin and within a "small" 25 cm × 25 cm detector of solid angle $\Delta\Omega$ were considered as "mono-energetic" and "mono-directional", with energy equal to the central value of each bin ($E = 1.5, 2.5, ..., 19.5$ GeV),

and direction aimed at the center of the "small" detector. Therefore, for each type of particle, the distribution that we calculated was the differential tracklength defined by

$$\frac{d^2L}{dEd\Omega}. \tag{A.2}$$

Figures A.1, A.2 and A.3 are the histograms of the tracklength distributions for the four central "small" detectors covering a total area of 50 cm × 50 cm.

Once the photon, electron and positron spectra in the beam dump were known, the mechanisms for production of X particles were considered. Axions can be produced by the following four processes: the Primakoff production of axions by photons[24]; "bremsstrahlung" of axions by electrons or positrons in the scattering process[25]; annihilation of a high energy positron and an atomic electron in the beam dump into a photon plus an axion; and the resonance production of the axion in the annihilation of a high energy positron and an atomic electron. Details of the production mechanisms are given below. Calculations for the first three production mechanisms can be carried out by the same procedure, we will describe them first. Discussion of the production of axions by resonance mechanism will follow afterwards.

The axion flux of the first three production processes were calculated by the following method. Using the production cross sections for the axion with a given mass, the energy spectrum of axions for each "small" detector was obtained for each "mono-energetic", "mono-directional" secondary beam (i.e. the beam of shower particles) by integrating over the total axion production solid angle $\Delta\Omega_X$ subtended by the "small" detector. This

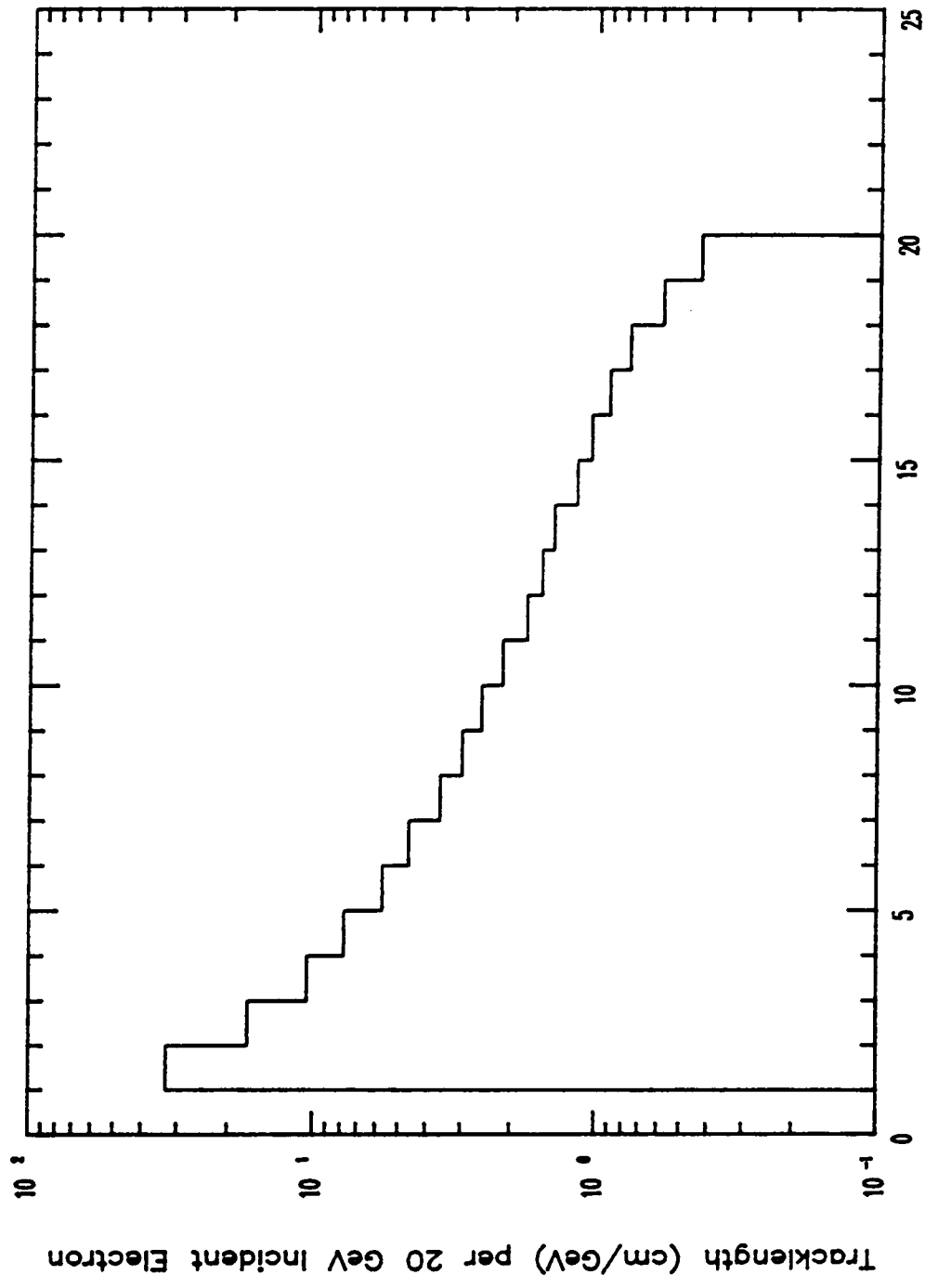

Figure A.1: Distribution of the photon tracklength of the electromagnetic shower, aiming at the 50*cm* × 50*cm* center area of the detector, produced by a 20 GeV electron interacting with the water.

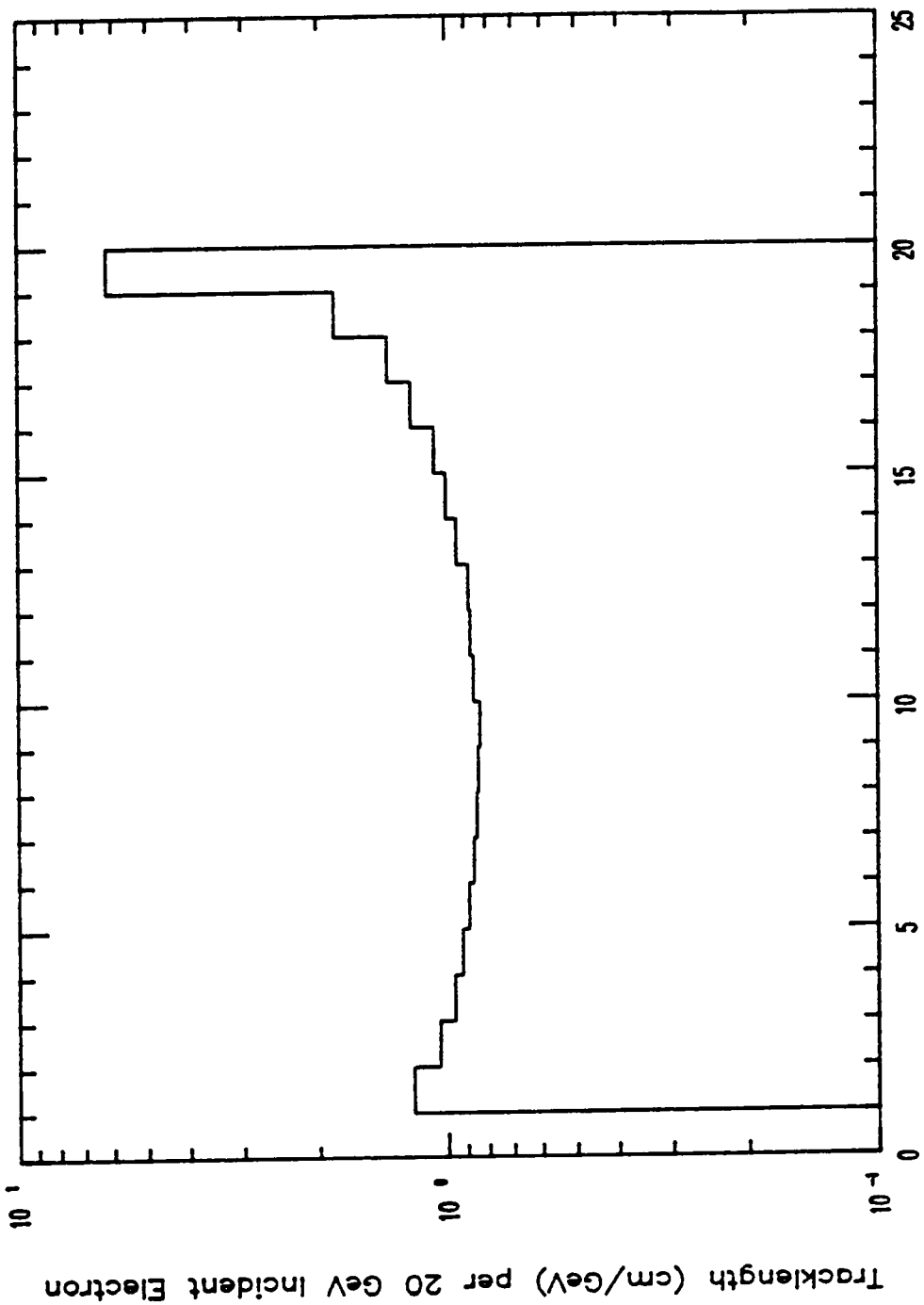

Figure A.2: Distribution of the electron tracklength of the electromagnetic shower, aiming at the 50*cm* × 50*cm* center area of the detector, produced by a 20 GeV electron interacting with the water.

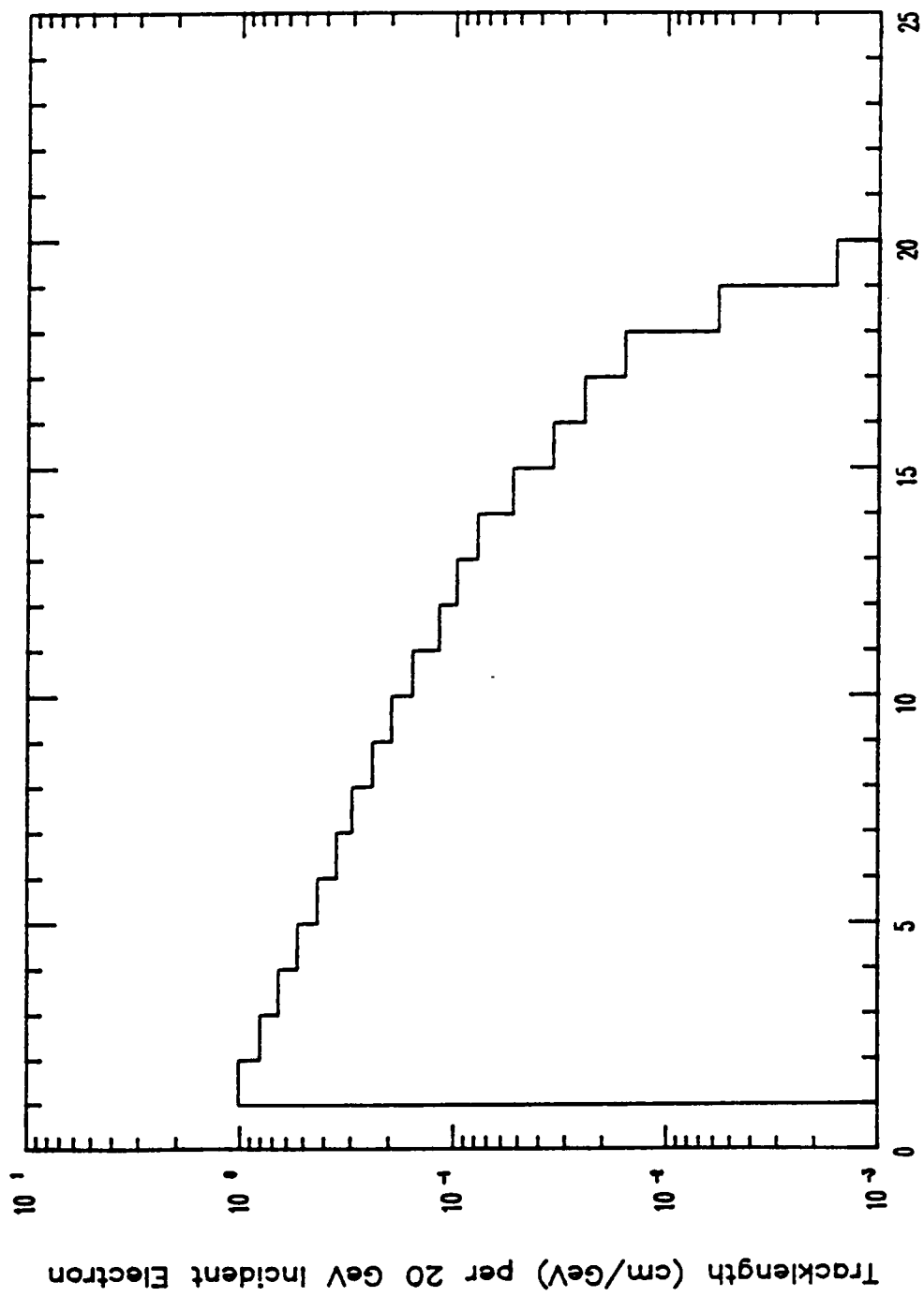

Figure A.3: Distribution of the positron tracklength of the electromagnetic shower, aiming at the 50*cm* x 50*cm* center area of the detector, produced by a 20 GeV electron interacting with the water.

integration was carried out by using a numerical integration subroutine. Summing over all the secondary beam directions (and energies in the case of bremsstrahlung production) we obtained the 144 axion energy spectra, one for each "small" detector, for each production process. The axion energy spectra were also sliced into $\Delta E_x = 1\ GeV$ bins, and for each "small" detector the axions within each energy bin ΔE_X were considered as "mono-energetic" and "mono-directional", with energy equal to the central value of each bin and directed at the center of the "small" detector. The minimum energy cut was 2 GeV and the axion energy E_X took the values of 2.5, 3.5, ..., 19.5 GeV. Since all the axion production cross sections are proportional to F_X^{-2}, this quantity was factored out. In other words, the axion energy spectra were calculated with $F_X = 1$.

The cross section for the Primakoff production mechanism is a function of both the axion production angle with respect to the photon direction and the photon energy. In the Primakoff mechanism, the axion energy is approximately equal to the photon energy. Therefore, we only need to sum over all the photon directions to get the desired axion flux. The differential axion flux is given by

$$\frac{d^2Flux(E_X,\Omega_X)}{dE_X d\Omega_X} = \frac{\rho}{A} N_A N \int d\Omega_\gamma \left(\frac{d^2L}{dE_\gamma d\Omega_\gamma}\frac{d\sigma}{d\Omega_X}\right), \qquad \text{(A.3)}$$

where $E_X = E_\gamma$, ρ is the density of the water, N_A is the Avogadro number, A is the molecular weight of water, $d\Omega_X$ is the differential solid angle for axion production, N is the total number of electrons in the primary beam, and L is the photon tracklength.

In the cross section for the Primakoff production mechanism, the form

factor of the target (which is a function of the four momentum transfer squared t) is involved. The quantity t represents the scale of the interaction. Depending upon the size of $t^{-1/2}$, either the atomic form factor or the nuclear form factor has to be used (note: t is defined as positive here). For example, for a distance corresponding to the Bohr radius ($\sim 0.53 \times 10^{-8}\ cm$), t is approximately equal to $1.6 \times 10^{-11}\ (GeV/c)^2$; for a distance corresponding to proton radius ($1.2 \times 10^{-13}\ cm$), t is approximately equal to $2.56 \times 10^{-2}\ (GeV/c)^2$. In the Monte-Carlo calculation, the form factor was switched from atomic form factor to nuclear form factor at $t = 3 \times 10^{-6}\ (GeV/c)^2$. This arbitrary division was just for the convenience of calculation, it did not introduce numerical error. The expressions for the form factor we used are given in Appendix B.

For a given secondary beam direction Ω_+ and energy E_+, the cross section for axion bremsstrahlung is a function of axion production angle Ω_X with respect to the secondary beam direction, and axion energy E_X. Therefore, we need to sum over all the secondary beam energies and directions to get the desired spectra. The differential distribution of axions is given by

$$\frac{d^2Flux(E_X,\Omega_X)}{dE_X d\Omega_X} = \frac{\rho}{A} N_A N \iint dE_+ d\Omega_+ \left(\frac{d^2L}{dE_+ d\Omega_+} \frac{d^2\sigma}{dE_X d\Omega_X}\right). \qquad \text{(A.4)}$$

In the above expression, L is the tracklength of either electron or positron.

In order to do the integration of the axion cross section over the axion solid angle, Ω_X, we had to calculate a function χ, which is related to the form factors, in terms of E_+, E_X, and θ_X. The expression for $\chi(E_+, E_X, \theta_X)$ is defined in Appendix B. For each E_+ and E_X, the function χ was calcu-

lated at 240 different θ_X values, ranging from 0 to DD/d, where DD is the diagonal dimension of the detector and d is the distance from the Beam Dump East to the detector. They were then interpolated into a continuous function of θ_X.

The annihilation production cross section is a function of the axion production angle, Ω^*, in the center of mass frame, and positron energy E_+. The axion energy E_X is determined by these two parameters. The expression for the differential axion flux is

$$\frac{d^2Flux(E_X,\Omega_X)}{dE_X d\Omega_X} = \frac{\rho}{A} N_e N N_e \int d\Omega_+ \left(\frac{d^2L}{dE_+ d\Omega_+}\frac{d\sigma}{d\Omega^*}\frac{dE_+}{dE_X}\frac{d\Omega^*}{d\Omega_X}\right), \qquad \text{(A.5)}$$

where $d\Omega^*$ is the differential solid angle for axion production in the center of mass frame, $d\Omega_X$ is the differential solid angle of the axion in the laboratory frame, N_e is the total number of electrons in one water molecule, and L is the positron tracklength distribution.

The final step was to consider the detection efficiencies for axions. The axions produced in the Beam Dump East were followed through the shielding (179.02 m long) and into the decay space (204.12 m long) in front of the detector. The efficiency for detecting an axion at a distance x from the beginning of the dump is the axion decay probability at x multiplied by the geometrical acceptance of the axion decay products. To a good approximation $x \ll \lambda$, where λ is the axion decay length, and therefoer the decay probability of an axion at distance x from the beginning of the dump is independent of the distance, and is given by

$$P(x)dx = \frac{dx}{\lambda}, \qquad \text{(A.6)}$$

If the axion decayed inside the dump and the earth shielding, the electrons and photons would be absorbed, resulting in zero detection efficiency. Neglecting the interaction of axions with the dump material, the detection efficiency η of an axion with given energy and mass becomes an integral of the geometrical acceptance $\eta'(E_X, x)$ over the axion decay vertex position x along the flight path in air. The flight path, l, is determined by the direction of the axion momentum. The efficiency is given by

$$\eta(E_X, \Omega_X) = \frac{1}{\lambda} \int_l dx \eta'(E_X, x). \tag{A.7}$$

Because of the collimation of the axion beam and the symmetry of the detector, it turned out that we have to calculate only the detection efficiency for axions aimed at the first half of the first quadrant of the detector, which is a triangle consisting of 21 "small" detectors. For each "small" detector, the detection efficiency for an axion aimed at the center was computed. In order to reduce the calculation time, we calculated only the geometrical acceptance at 75 positions along a flight path, i.e., the integration was reduced to a summation of the 75 values. For axion decaying into electrons, the efficiencies were calculated at nine different axion masses, ranging from 1.1 MeV/c^2 to 200 GeV/c^2, and at 12 different axion energies, ranging from 2 GeV to 19.5 GeV. Using the Lagrangian interpolation procedure, the detection efficiency was made into a continuous function of the axion energy. Noticing that for the axion decaying into two photons, the efficiency is in fact a function of $\gamma = E_X/m_X$. Efficiencies were calculated at 112 different values of γ, ranging from 2 to 10^{30}. The Lagrangian interpolation method was also used to make the efficiency into a continuous function of

γ. At a later stage, when combining the axion flux with the efficiency to obtain the event rate, the values of γ were translated into the axion energy for each fixed axion mass.

For a given position on a flight path, the geometrical acceptance of an axion is defined as the probability of detecting at least one of the decay products. In the center of mass frame, the electron-positron pair or two photons from the axion decay have the momenta equal in magnitude, but in opposite directions. When they are Lorentz transformed into the laboratory frame, their polar angles, θ_1 and θ_2, are different from the values in the center of mass frame, but their azimuthal angles, ϕ and $\phi + \pi$, remain the same. Therefore, two decay products of the axion were described by two concentric circles in the detector plane, with their radii given by

$$r_1 = R\theta_1, \quad and \quad r_2 = R\theta_2, \tag{A.8}$$

where R is the distance from the axion decay vertex position to the detector plane. We calculated the percentages of the circumferences of these two circles lying outside the detector. The product of these two percentages was taken as the probability for detecting zero axions, P_{no}. The geometrical acceptance for detecting an axion is given by

$$P(\theta^*) = 1 - P_{no}(\theta^*), \tag{A.9}$$

where θ^* is the polar angle of one of the decay product in the center of mass frame. The value of θ^* was generated by a random number generator which was evenly distributed between 0 and π. The generator was called

75 times for each axion decay position. The final value of the geometrical acceptance was obtained by averaging the 75 different values of $P(\theta^*)$.

Since the efficiency is proportional to λ^{-1}, (which is proportional to F_X^{-2}), the dependance of F_X was factored out in the calculation. For an axion with a given mass, the event rate in the "small" detector was the summation of the products of the axion flux and the detection efficiency at different axion energies, E_X. The total event rate was obtained by summing up the rates for all 144 "small" detectors. It is given by

$$rate = \iint dE_X d\Omega_X [\frac{d^2 Flux(E_X, \Omega_X)}{dE_X d\Omega_X} \eta(E_X, \Omega_X)]. \qquad (A.10)$$

The dependance of the rate on the axion decay constant F_X was reintroduced by multiplying the final result by a factor F_X^{-4}.

For axions decaying into two photons, the event rates were calculated at 13 different mass values, ranging from 50 KeV/c^2 to 200 MeV/c^2. For axions decaying into an electron-positron pair, the event rates at nine different mass values were calculated, ranging from 1.1 MeV/c^2 to 200 MeV/c^2.

To calculate the total cross section for axion resonance production in the annihilation of a positron with an atomic electron, the Breit-Wigner resonance formula was used. The cross section is a function of the axion energy E^* in the center of mass frame. Since the axion decay width is much smaller than the step size of E^*, the total cross section was taken as a delta function,

$$\sigma(E^*) = (Area)_0 \delta(E^* - m_X), \qquad (A.11)$$

where $(Area)_0$ is the energy integral of the cross section. For a given axion mass, we have a mono-energetic axion flux over the entire positron energy

range. The differential axion flux is given by

$$\frac{dFlux(\Omega_X)}{d\Omega_X} = \frac{\rho}{A} N_A N_e \frac{d^2L}{dE_+ d\Omega_+} \frac{dE_+}{dE^*} (Area)_0, \qquad (A.12)$$

where the positron energy has the value

$$E_+ = \frac{m_X^2 - m_e^2}{2m_e}. \qquad (A.13)$$

The cross section is also proportional to the F_X^{-2}, which was factored out in the calculation.

The annihilation of high energy positrons with atomic electrons in the beam dump may also produce photinos through the exchange of a selectron[36]. Details of the photino production mechanism are given below. The photino production cross section is a function of the positron energy, E_+, and the photino production angle, θ^*, in the center of mass frame. The photino spectrum was calculated in exactly the same way as that for the axions production process by electron and positron annihilation, except that the photino production cross section is proportional to $m_{\tilde{e}}^{-4}$ ($m_{\tilde{e}}$ is the mass of selectron). Since the photino decays into a goldstino and a photon[35], and only the photon can be detected, the geometrical acceptance for the photino is defined as the probability of observing a photon from the decay of a photino in flight. The geometrical acceptance for a photon from the photino decay is calculated by a procedure similar to that of axion. The minimum energy cut for the photon was 2 GeV. The detection efficiency was calculated at 11 different values of photino mass, $m_{\tilde{\gamma}}$, ranging from 100 KeV/c^2 to 65 MeV/c^2; and at 12 different values of positron energy,

ranging from 2.0 to 19.5 GeV. To first order the detection efficiency is proportional to the parameter, d^{-2}, and it was factored out.

Finally, the photino flux was folded in with the detection efficiency to arrive at the event rate. The event rates were calculated at 11 different values of photino mass, ranging from 100 KeV/c^2 to 65 MeV/c^2. Also the event rates were parametrized by two quantities unknown yet, the $m_{\tilde{\gamma}}$ and the supersymmetry breaking scale $d^{1/2}$. The dependance on the two parameters take the form of multiplicative factor.

The axion (photino) event rate calculated here was the average number, $\overline{n}$, of axions (photinos) that could be detected in the beam dump experiment. In principle, the number of axions that can be detected in an experiment has a Poisson distribution, if the event rate is small. The probability of detecting n axions in one experimental run is given by

$$P_{\overline{n}}(n) = \frac{\overline{n}^n}{n!} e^{-\overline{n}}, \quad n = 0, 1, 2, ..., \tag{A.14}$$

and the average number, $\overline{n}$ can be obtained by running the experiment many times. From one experimental run we do not have enough information to get the distribution of n, to determine $\overline{n}$ with certainty. However, we can find an upper bound $\overline{N}$ that the true value of $\overline{n}$ will lie in the region $(0, \overline{N})$ with a specified high probability (confidence level) $1 - \alpha$. The upper bound $\overline{N}$ is determined by the equation,

$$1 - \alpha = 1 - \sum_{n=0}^{n_0} P_{\overline{N}}(n), \tag{A.15}$$

where n_0 is the number particles detected in an experiment. In this experiment no candidate event was found, therefore $n_0 = 0$. This leads to the

upper bound $\overline{N} = 3$ at 95% confidence level. Since $F_X^{-4} \propto \bar{n}$ for the axion, and $d^{-2} \propto \bar{n}$ for the photino, this limit was translated into a lower limit for F_X and $\sqrt{d}$ at 95% confidence level. They are shown in Figures IV.2, IV.3 and IV.9.

The formulae used for calculating various production processes are summarized in Appendix B.

Appendix B

Formulae Used in Event Rate Calculations

B.1 Primakoff Production

The Feynman diagram for the Primakoff production mechanism is shown in Figure IV.1(a). The cross section for the photo-production of axions via the Primakoff mechanism[24] is given by

$$\frac{d\sigma}{d\Omega} = 8\alpha\frac{\Gamma}{m_X^3} \mid F(t) \mid^2 \frac{\theta^2}{(\theta^2+\delta^2)^2}, \tag{B.1}$$

where Γ is the axion decay width, $F(t)$ is the form factor of the target, θ is the axion production angle with respect to the photon direction, and t is the four momentum transfer squared, approximately given by

$$t \approx E_\gamma^2(\theta^2+\delta^2), \tag{B.2}$$

where the parameter δ is defined by

$$\delta = \frac{1}{2}\frac{m_X^2}{E_\gamma^2}.$$

Also to a first order approximation, the axion energy can be approximated by

$$E_X \approx E_\gamma. \tag{B.3}$$

Because the axion is predominantly produced with the low momentum transfer of the target, it suffices to consider only the atomic form factor and the nuclear elastic scattering form factor. For $t \leq 3 \times 10^{-6}\ (GeV/c)^2$, the atomic form factor[47] was used. It is given by

$$\mid F(t) \mid^2 = Z^2(\frac{a^2t}{a^2t+1})^2 + Z(\frac{a'^2t}{a'^2t+1})^2, \tag{B.4}$$

where for hydrogen,

$$a = \frac{122.8}{m_e}, \qquad a' = \frac{282.4}{m_e},$$

and for oxygen,

$$a = 111\frac{Z^{-1/3}}{m_e}, \qquad a' = 773\frac{Z^{-2/3}}{m_e}.$$

For $t > 3 \times 10^{-6}\ (GeV/c)^2$, the elastic nuclear form factor was used. For protons, the electric dipole form factor was used[47]. It is given by

$$F(t) = (1 + \frac{t}{0.71})^{-2}. \tag{B.5}$$

For oxygen nucleus, the form factor is given by[48]

$$F(t) = Z(1 - \frac{a_0^2t}{8})e^{-a_0^2t/4}, \tag{B.6}$$

where $a_0 = 8.79\ (GeV/c)^{-1}$, and t is in the unit of $(GeV/c)^2$.

B.2 "Bremsstrahlung" of Axion in Electron Scattering

When an electron (or a positron) is scattered from nuclear targets the axion can be "bremsstrahlunged" from an electron (or positron)[25]. The

Feynman diagram for this process is shown in Figure IV.1(b). The cross section is given by

$$\frac{d^2\sigma(E_+, E_X, \theta_X)}{dE_X d\Omega_X} = \frac{\alpha^2\alpha_e}{\pi}\frac{E_+}{U^2}\chi\{x^3 - \frac{2m_X^2x^2(1-x)}{U} + \frac{2m_X^2}{U^2}[m_X^2x(1-x)^2 + m_e^2x^3(1-x)]\}, \quad \text{(B.7)}$$

where E_+ is the incoming electron or positron energy, E_X is the outgoing axion energy, θ_X is the angle between the axion and the electron (positron) directions, χ is used to calculate the photon flux in the one-photon-exchange approximation process, and

$$\begin{aligned} \alpha_e &= \frac{1}{4\pi}(\frac{m_e}{F_X})^2, \\ x &= \frac{E_X}{E_+}, \\ U &= E_+^2x\theta^2 + m_e^2x + \frac{m_X^2(1-x)}{x}. \end{aligned}$$

The function χ is related the structure functions, W_1 and W_2, of the target in the deep inelastic electron scattering[47]. At low momentum transfer, the electron scattering process can be regarded as photo-production reaction. The "equivalent" photon flux can be approximated by that produced by an electron passing through a "virtual" radiator of thickness $(3/4)(\alpha/\pi)\chi$ r.l. The expression for χ is given by

$$\chi = \int_{t_{min}}^{t_{up}} dt \mid F(t) \mid^2 \frac{t - t_{min}}{t^2}, \quad \text{(B.8)}$$

where t_{min} is the minimum value of the four momentum transfer squared as given by

$$t_{min} = (\frac{U}{2E_+(1-x)})^2, \quad \text{(B.9)}$$

and t_{up} is the upper limit of the integration. In the event rate calculation, we have used

$$t_{up} = \frac{U}{1-x}. \tag{B.10}$$

This simply provides a way of reducing the computation time on the computer, since the nuclear form factor decreases very rapidly at large values of t. The value of t_{up} is the same as that used in reference [25] to obtain equation [21]. The function χ is divided into two parts,

$$\chi = \chi_1 + \chi_2, \tag{B.11}$$

where χ_1 is related to the atomic form factor, $F(t)$, and is given by

$$\chi_1 = \int_{t_{min}}^{t_1} dt \mid F(t) \mid^2 \frac{t - t_{min}}{t^2}. \tag{B.12}$$

Here t_1 is equal to either t_{up} or 3×10^{-6} $(GeV/c)^2$ depending upon which one is smaller. The function χ_2 is nonzero only when t_{up} is greater than t_1. It is related to the nuclear form factor. For proton, χ_2 is defined as

$$\chi_2 = \int_{t_1}^{t_{up}} \frac{dt}{t^2} \frac{(t - t_{min})[1 + \tau(\mu_p^2 - 1)] + 2t_{min}\tau\mu_p^2}{(1 + t/0.71)^4} \tag{B.13}$$

where $\mu_p = 2.793$ is the anomalous magnetic moment of proton and $\tau = t/(4m_p^2)$. For oxygen nucleus, χ_2 is equal to either χ^{el} or χ^{quasi} depending upon which one is bigger. The quantity χ^{el} is related to elastic nuclear form factor of oxygen, $F(t)$, as given by

$$\chi^{el} = \int_{t_1}^{t_{up}} dt \mid F(t) \mid^2 \frac{(t - t_{min})}{t^2}. \tag{B.14}$$

The quantity χ^{quasi} is related to the quasi elastic nuclear form factor of oxygen,

$$\chi^{quasi} = \int_{t_1}^{t_{up}} dt \frac{C(t)}{(1+t/0.71)^4}\{(t-t_{min})[Z\frac{1+\mu_p^2\tau}{1+\tau} + (A-Z)\mu_n^2\frac{\tau}{1+\tau}] + 2t_{min}[2\mu_p^2\tau + (A-Z)\mu_n^2\tau]\} \quad \text{(B.15)}$$

where $\mu_n = 1.91$, and it is the anomalous magnetic momentum of neutron, and $C(t)$ is the Pauli "suppression" factor as given by

$$C(t) = \begin{cases} 1 & \text{if } Q > 2P_f, \\ \frac{3}{4}\frac{Q}{P_f}[1 - \frac{1}{12}(\frac{Q}{P_f})^2] & \text{otherwise.} \end{cases}$$

In the above expression,

$$Q = \frac{t^2}{(2m_p)^2} + t,$$

and $P_f = 0.25\ GeV$.

B.3 Production of Axion by Electron and Positron Annihilation: $e^+ + e^- \rightarrow X + \gamma$

The Feynman diagram for the production of axions by electron and positron annihilation is shown in Figure IV.1(c). The cross section is given by

$$\frac{d\sigma}{d(\cos\theta^*)} = \frac{1}{2}g^2\alpha\frac{1}{S}(\frac{m_X^2}{S-m_X^2})[(1-\beta\cos\theta^*)(1+\beta\cos\theta^*)]^{-1}, \quad \text{(B.16)}$$

where $g = m_e/F_X$, S is the center of mass energy squared and is given by

$$S = 2E_+m_e + 2M_e^2, \quad \text{(B.17)}$$

θ^* is the polar angle of the axion in the center of mass frame, and

$$\beta \approx 1 - 2\frac{m_e^2}{S}.$$

The axion energy in the laboratory frame can be expressed as

$$E_X = \frac{1}{4m_e}[(S + m_X^2) + (S - m_X^2)\beta \cos\theta^*]. \tag{B.18}$$

This cross section has an infrared divergence. Therefore, a low energy cut of 3 MeV was applied to the photon in the center of mass frame in order to avoid this difficulty.

B.4 Resonance Production of Axion in Electron and Positron Annihilation

The Feynman diagram for resonance production of axions in electron and positron annihilation is shown in Figure IV.1(d). The Breit-Wigner resonance formula was used to calculate the total cross section. It is given by

$$\sigma(E^*) = \sigma_{max}\frac{\Gamma^2/4}{(E^* - m_X)^2 + \Gamma^2/4}, \tag{B.19}$$

where E^* is the axion energy in the center of mass frame; m_X, the axion mass; Γ, the total axion decay width is given by

$$\Gamma = \Gamma_{X\to e^+e^-} + \Gamma_{X\to\gamma\gamma}, \tag{B.20}$$

and σ_{max}, the peak cross section whose value depends on the particular axion decay channel being considered. For an axion decaying into two photons, the cross section is expressed as the following equation,

$$\sigma_{max} = \frac{4\pi}{E^{*2}}\frac{(2J+1)}{(2s_a+1)(2s_b+1)}\frac{\Gamma_{X\to e^+e^-}\Gamma_{X\to 2\gamma}}{\Gamma^2}, \tag{B.21}$$

where J is the axion spin (which is equal to 0); s_a and s_b, the spins of electron and positron, respectively. For an axion decaying to an electron and a positron, it is defined as,

$$\sigma_{max} = \frac{4\pi}{E^{*2}} \frac{(2J+1)}{(2s_a+1)(2s_b+1)} \frac{\Gamma^2_{X\to e^+e^-}}{\Gamma^2}. \tag{B.22}$$

The axion energy in the laboratory frame is given by

$$E_X = E_+ + m_e, \tag{B.23}$$

where E_+ is the positron energy. The axion energy in the center of mass frame is given by

$$E^* = \sqrt{2m_e E_+ + m_e^2}. \tag{B.24}$$

The total cross section is given by

$$\begin{aligned} (Area)_0 &= \int_{-\infty}^{\infty} dE^* \sigma(E^*) \\ &= \frac{\pi}{2} \Gamma \sigma_{max}. \end{aligned} \tag{B.25}$$

B.5 Production of Photino Pairs

The photino pair can be produced by a high energy positron from the electromagnetic shower inside the dump interacting with an atomic electron[36]. The Feynman diagram is shown in Figure IV.1(e). The cross section is given by

$$\frac{d\sigma}{d\Omega^*} = \frac{\alpha^2 S}{4m_{\tilde{e}}^4}(1+\cos^2\theta^*_{\tilde{\gamma}})\beta^3, \tag{B.26}$$

where $m_{\tilde{e}}$ is the selectron mass; β, the P-wave factor, is defined by

$$\beta = (1 - \frac{4m_{\tilde{\gamma}}^2}{S})^{1/2}, \tag{B.27}$$

and S, the center of mass energy squared given by

$$S = 2E_+ m_e + m_e^2. \tag{B.28}$$

The photino energy in the laboratory frame is given by

$$E_{\tilde{\gamma}} = \frac{S}{4m_e}(1 + \beta(1 - \frac{4m_e^2}{S})^{1/2} \cos\theta^*_{\tilde{\gamma}}). \tag{B.29}$$

B.6 The Decay Probability of the Axion and Photino

If the axion like particle decays into two photons, its lifetime is given by[1]

$$\tau_{X\to 2\gamma} = \frac{64\pi^3}{\alpha^2}\frac{F_X^2}{m_X^3}, \tag{B.30}$$

where F_X is the decay coupling constant; and if it is heavier than two electron masses, then the axion should also decay into an electron-positron pair with the lifetime given by[1]

$$\tau_{X\to e^+e^-} = \frac{8\pi F_X^2}{m_e^2(m_X^2 - 4m_e^2)^{1/2}}. \tag{B.31}$$

If a photino decays into an electron and a goldstino, the lifetime is given by[35]

$$\tau_{\tilde{\gamma}\to\tilde{g}+\gamma} = \frac{8\pi d^2}{m_{\tilde{\gamma}^s}}, \tag{B.32}$$

where $\sqrt{d}$ is the supersymmetry breaking scale.

The decay length, λ, is defined as

$$\lambda = \frac{P_X}{m_X} c\tau, \tag{B.33}$$

where P_X is the momentum in the laboratory frame. The decay probability of an X particle at a distance, x, from the beginning of the Beam Dump East is given by

$$P(x)dx = \frac{dx}{\lambda}e^{-x/\lambda}. \tag{B.34}$$

Since no event was observed in this experiment, the decay length of an axion could be much longer than the distance between the detector and the beginning of the Beam Dump East, $x/\lambda \ll 1.0$; therefore the approximation,

$$P(x)dx \approx \frac{dx}{\lambda}, \tag{B.35}$$

is adequate, and it permits us to factor out the decay coupling constant, F_X, in the rate calculations.

B.7 Lifetime of the PQWW Axion

For the PQWW axion, with mass in the range from 100 KeV/c^2 to 400 KeV/c^2, the lifetime is given by[8,9,12]

$$\tau_{a\to 2\gamma} = \tau_{\pi^0\to 2\gamma}(\frac{m_\pi}{m_a})^5\frac{1}{z}, \tag{B.36}$$

where z is the ratio of the u quark mass to that of the d quark; $\tau_{\pi^0\to 2\gamma}$, the neutral pion lifetime, given by

$$\tau_{\pi^0\to 2\gamma} = \frac{64\pi^3}{\alpha^2}\frac{f_\pi^2}{m_\pi^3}; \tag{B.37}$$

and f_π, the pion decay constant. The axion mass is given by

$$m_a = m_\pi(\frac{f_\pi}{f_a})N(x+\frac{1}{x})\frac{z^{1/2}}{1+z}, \tag{B.38}$$

where x is the ratio of the vacuum expectation values of the "Higgs" scalar fields, and N is the number of quark families. Combining equations B.36, B.37, and B.38, we can relate the lifetime of the PQWW axion and the lifetime of the axion-like particle by the following expression,

$$\tau_{a\to 2\gamma} = \tau_{X\to 2\gamma}\frac{1}{N^2}\frac{x^2}{(1+x)^2}\frac{(1+z)^2}{z^2}. \tag{B.39}$$

In the rate calculations, the values used are $N = 3, z = 0.56$[49], and $x = 1$.

The vita has been removed from the scanned document